J Polym Eng 31 (2011): 495–519 © 2011 by Walter de Gruyter • Berlin • Boston. DOI 10.1515/POLYENG.2011.095

Strain localization in polycarbonates deformed at high strain rates

Anoop G. Varghese and Romesh C. Batra*

Department of Engineering Science and Mechanics, M/C 0219, Virginia Polytechnic Institute and State University, Blacksburg, VA 24061, USA, e-mail: rbatra@vt.edu

*Corresponding author

Abstract

We studied three-dimensional transient large coupled thermo-mechanical deformations of a polycarbonate (PC) plate with a through-the-thickness inhomogeneity at its centroid. The PC exhibits strain softening followed by strain hardening and its elastic moduli are taken to be functions of strain rate and temperature. The inhomogeneity is either a void or a region of initial temperature higher than that of the rest of the plate. The nonlinear initial-boundary-value problem is solved numerically by the finite element method. It is found that deformations localize into narrow regions that we call bands. For a plate deformed in tension, the maximum principal stretch within the band is almost twice that of the maximum shear strain and for a plate deformed in shear the two have approximately the same magnitude. For the PC deformed in uniaxial compression, we call the minimum slope of the effective stress vs. the effective strain curve in the strain softening regime as the softening modulus, E_s, and find values of E_s and the defect strength needed for the deformations to localize. These values are found to be different for the plate deformed in shear from that deformed in tension and the minimum value of E_s for the localization of deformation also depends upon the defect type and the defect strength (e.g., the ratio of the major to the minor axes of the elliptic void).

Keywords: coupled large transient thermo-mechanical deformations; finite element solution; polycarbonate; strain localization.

1. Introduction

The thermo-mechanical response of a polycarbonate (PC) is different from that of a metal and a metallic alloy due to differences in their atomic structures. Polymers are usually comprised of long chains of monomers [1] and metals of grains with each grain being a single crystal. A typical experimental true axial stress vs. true axial strain curve of a PC in glassy state deformed in uniaxial compression at different strain rates is shown in Figure 1. Young's modulus and the flow stress of a PC usually depend upon the strain rate and the temperature; the flow stress also depends on the hydrostatic pressure [3]. The post yield response is characterized by intrinsic strain softening during which the true axial stress decreases with an increase in the true axial strain and it is followed by strain hardening [4].

The strain softening (hardening) of a material point usually destabilizes (stabilizes) deformations. Several investigators have observed instabilities during large deformations of a PC in the form of narrow bands or necking (e.g., see [5, 6]). In PCs, the extent of the strain localized region might be limited because of the hardening of the material following its softening. Wu and Turner [7] experimentally studied torsional deformations of tubular PC specimens, observed instabilities after the material had yielded and found that the maximum shear strain within the band reached 70% at the fully softened stage and remained constant thereafter. During simple shearing deformations of a PC specimen, G'Sell and Gopez [8] observed a band of localized deformation triggered by an existing inhomogeneity in the material, and the band widened along lines perpendicular to the direction of the applied shear; a similar phenomenon has been reported in [5, 9].

Strain localization in PCs has also been investigated numerically, e.g., see [9–13]. Grenet and G'Sell [10] have studied quasi-static shearing deformations of a PC plate with a defect near its centroid. Many features of the localization of deformation observed experimentally were well captured during simulations using a one dimensional (1D) constitutive equation. Wu and van der Giessen [12] analyzed plane strain quasi-static simple shearing deformations of a PC using the finite element method (FEM) and constitutive relations similar to those proposed by Boyce et al. [14]. Their constitutive equations can reproduce the mechanical response of PCs over a wider range of temperatures and strain rates than those used by Grenet and G'Sell [10]. Wu and van der Giessen [12] introduced a weak region within the specimen that served as the nucleation site for the deformations to localize and found that the intrinsic strain softening was the driving force for the shear band formation and they did not observe a shear band in the limiting case of no strain softening. They [15] also studied necking of a PC dog bone sample deformed in quasi-static plane strain tension, which successfully predicted various stages of necking observed in experiments and concluded that strain softening was the driving force for necking. Lu and Ravi-Chandar [11] studied both experimentally and numerically the shear band formation in a PC specimen deformed in uniaxial tension. Experimental observations revealed micro shear bands in the material, particularly near surface defects, which grew with the deformation. For numerical simulations of quasi-static deformations of a rectangular specimen deformed in simple tension, the true axial stress vs. the true

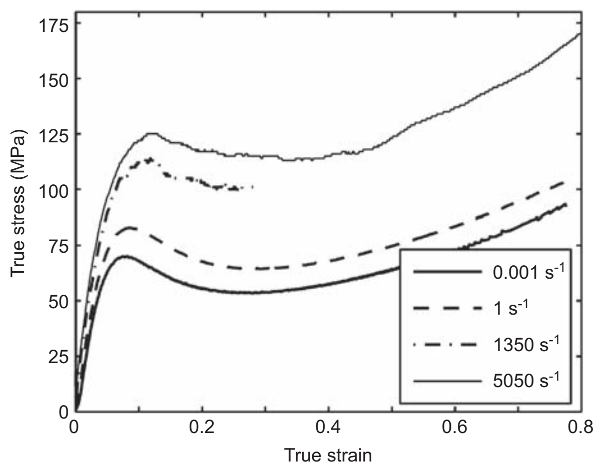

Figure 1 True axial stress vs. the true axial strain curves for a PC deformed in uniaxial compression at various strain rates (from Mulliken and Boyce [2]).

axial strain curve of the PC was idealized by a trilinear curve with linear portions corresponding to elastic, yielding, and strain hardening regimes of deformation. Neither the test data nor the idealized stress-strain curve had any strain softening regime. They found that localized regions of high plastic strain formed and propagated within the material and they called them shear bands, and concluded that strain softening is not the driving mechanism for the shear band formation in a PC. Effects of loading rate, temperature and the dependence of the yield stress upon the hydrostatic pressure were ignored.

Sweeney et al. [16] found that depending on the polymer, the region of localized deformation could take different geometrical forms like a shear band or necking in a dog bone sample. They developed constitutive equations for a PC by assuming each material point to have two phases connected in series: an Eyring process and a Gaussian network. The strain localized region took the form of a shear band when the Gaussian network was stiff and the Eyring process dominated, and a symmetric neck when the Gaussian network was relatively soft. The dominance of a phase is determined after finding values of material parameters that fit the experimentally obtained stress-strain curve. The PC dog bone samples were tested in tension at an axial strain rate of ~0.07/s and a temperature of 373 K. Sweeney et al. [16] predicted the occurrence of a shear band or of a necking instability but analyzed neither the propagation nor the speed of a shear band.

Govaert et al. [17] studied quasi-static tensile and torsional deformations of circular cylindrical PC dog bone specimens deformed at low strain rates, observed zones of localized deformations and showed that the strain softening in PCs could be suppressed by cyclically twisting PC samples prior to testing them in uniaxial tension and torsion. They found that strain localization occurred only in those materials that exhibited strain softening, which seemingly contradicts Lu and Ravi-Chandar’s [11] findings. Results of their numerical simulations employing a compressible Leonov model that can reproduce the strain softening and the strain hardening phenomena in PCs agreed with their experimental observations. Even though they showed that the strain softening is necessary for the strain localization to occur, the minimum strain softening needed for the strain localization to occur was not quantified.

Although several investigators have shown that deformations can localize in PCs under quasi-static loading, very little work has been done on studying the deformation localization phenomenon at high strain rate deformations of PCs. An understanding of this phenomenon will help design industrial processes such as extrusion, drawing and molding wherein the material undergoes large plastic deformations. Instabilities occurring in these processes will very likely generate defects in fabricated parts and make them either partially or fully useless. This work will help quantify processing parameters so that instabilities either do not occur or are minimized. It will also help characterize materials that are resistant to fragmentation under impact loading, e.g., a stone striking automobile’s windshield.

The objectives of this work are to delineate the effect on the strain localization of (i) high strain rates of deformations, (ii) strain softening and quantify, if possible, the minimum softening needed for the region of strain localization to propagate, (iii) initial defect in the form of an elliptic void and (iv) a zone of elevated initial temperature. We propose a criterion for the deformation localization, compute the speed of propagation of this band and find if either the maximum principal stretch or the maximum shear strain at points within the band has high values. In addition to the material softening, the initiation of deformation localization depends upon the number, the type and the strength of defects present in the body. Generally speaking, a geometric singularity (e.g., a void, a crack or a notch) facilitates the initiation of localization of deformation more than a material inhomogeneity and thus a precise answer to the afore-stated objectives cannot be obtained.

We accomplish these goals by studying (i) three-dimensional (3D) deformations of a square PC plate with either a through-the-thickness elliptic hole at its centroid or a circular region of elevated temperature and deformed by pulling axially the two opposite edges with the other two edges kept traction free and (ii) plane strain shearing deformations of a PC specimen with a defect at its centroid that is initially at a temperature higher than that of the rest of the body.

It is found that in the region of localization, principal stretches rather than the maximum shear strain dominate. However, in PC specimens deformed in simple shear, the two strains are nearly of the same order of magnitude. The minimum value of the softening modulus, defined as the minimum slope of the magnitude of the Cauchy stress tensor vs. the magnitude of the true strain tensor curve in the strain softening regime during uniaxial compressive deformations, required for deformations to localize is found to depend upon the type and the strength of the defect in addition to the type of deformation. For a strong enough defect, deformations localize in the absence of the PC exhibiting any strain softening.

AUTHOR’S COPY | AUTORENEXEMPLAR

The rest of the paper is organized as follows. The problems are formulated in Section 2, constitutive relations for a PC for its high strain rate thermo-mechanical deformations are briefly reviewed in Section 3 and the deformation localization criterion is stated in Section 4. Section 5 describes the numerical scheme used to find an approximate solution of the nonlinear coupled multiphysics (mechanical and thermal deformation) initial-boundary-value (IBV) problem formulated in Sections 2 and 3. Section 6 gives results of numerical simulations and conclusions of the work are summarized in Section 7.

2. Problem formulation

2.1. Plate with a through-the-thickness elliptic void

A schematic sketch of the problem involving a square plate composed of a homogeneous and isotropic PC and having a through-the-thickness elliptic hole at the plate centroid is depicted in Figure 2. The plate is deformed by pulling axially its top and bottom surfaces with a speed that increases linearly from zero to a steady value in time t^0. The order of singularity in deformations at the geometric imperfection depends upon the ratio of the lengths of the major and the minor axes of the elliptic void and the orientation of the void relative to the direction of loading, and will very likely affect when deformations localize.

In the Lagrangian description of motion balance laws governing deformations of the plate material are:

$$\text{Mass: } \rho J=\rho_0 \text{ in } \Omega \tag{1}$$

$$\text{Linear momentum: } \rho_0\dot{\mathbf{v}}=\nabla\cdot\hat{\mathbf{T}} \text{ in } \Omega \tag{2}$$

$$\text{Moment of momentum: } \hat{\mathbf{T}}\mathbf{F}^T=\mathbf{F}\hat{\mathbf{T}}^T \text{ in } \Omega \tag{3}$$

$$\text{Energy: } \rho_0 c\dot{\theta}=\dot{Q} \text{ in } \Omega \tag{4}$$

Here, ρ_0 and ρ are mass densities in the reference and the current configurations, respectively, $J=\det \mathbf{F}$ is the Jacobian, $\mathbf{F}=\partial\mathbf{x}/\partial\mathbf{X}$ the deformation gradient where $\mathbf{x}$ and $\mathbf{X}$ are coordinates of places a material particle occupies in the deformed and the undeformed configurations, respectively, θ the temperature, c the specific heat, $\dot{Q}$ the heating produced per unit volume in the reference configuration due to plastic working, $\mathbf{v}$ the velocity field defined as $\mathbf{v}=\dot{\mathbf{x}}$, and a superimposed dot denotes the material time derivative. Furthermore, $\hat{\mathbf{T}}$ is the first Piola-Kirchhoff stress tensor and $\nabla\cdot\hat{\mathbf{T}}$ the divergence of $\hat{\mathbf{T}}$ with respect to coordinates in the reference configuration. The first Piola-Kirchhoff stress tensor is related to the Cauchy stress tensor, $\boldsymbol{\sigma}$, by $\hat{\mathbf{T}}=J\boldsymbol{\sigma}(\mathbf{F})^{-T}$. In Eq. (4), we have assumed that effects of heat conduction are negligible, i.e., deformations are locally adiabatic. Batra and Kim [18] have shown that in metallic bodies deformed at high strain rates the thermal conductivity does not affect the time of initiation of the localization of deformation but influences the band width; it is tacitly assumed that the same conclusion can be carried over to a PC.

The body is assumed to be initially at rest, stress free and at a uniform temperature of 300 K.

Because of the symmetry of the plate geometry, the void and of the initial and the boundary conditions about the three centroidal planes we assume that plate's deformations are symmetric about the X_1-, the X_2- and the X_3-axes shown in Figure 2. Accordingly, we analyze deformations of one-eighth of the plate in Figure 2 (shown in grey) under the following boundary conditions:

$$x_1=0 \quad \bar{t}_2=0 \quad \bar{t}_3=0 \quad \text{on } X_1=0 \tag{5a}$$

$$\bar{t}_1=0 \quad \bar{t}_2=0 \quad \bar{t}_3=0 \quad \text{on } X_1=L \tag{5b}$$

$$x_2=0 \quad \bar{t}_1=0 \quad \bar{t}_3=0 \quad \text{on } X_2=0 \tag{5c}$$

$$x_3=0 \quad \bar{t}_1=0 \quad \bar{t}_2=0 \quad \text{on } X_3=0 \tag{5d}$$

$$\bar{t}_1=0 \quad \bar{t}_2=0 \quad \bar{t}_3=0 \quad \text{on } X_3=h/2 \tag{5e}$$

$$v_2=\begin{cases} v_0\dfrac{t}{t^0}, & 0\le t<t^0 \\ v_0, & t\ge t^0 \end{cases} \quad \bar{t}_1=0 \quad \bar{t}_3=0 \quad \text{on } X_2=L \tag{5f}$$

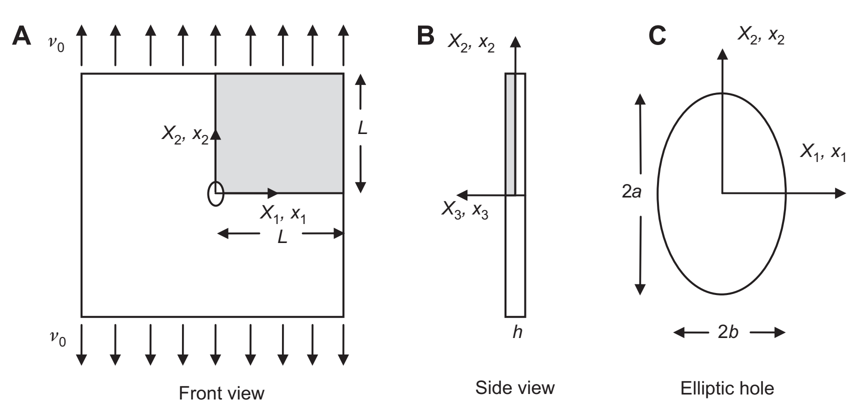

Figure 2 (A) Front and (B) side views of a square plate with a through-the-thickness void and (C) shape of the elliptic void.

$$\hat{T}_{i\beta}N_{\beta}=0\ \ (i=1,2,3;\beta=1,2)\ \ \text{on}\ \left(\frac{X_1}{b}\right)^2+\left(\frac{X_2}{a}\right)^2=1 \tag{5g}$$

Here, $\bar{\mathbf{t}}=\hat{\mathbf{T}}\mathbf{N}$ is the present traction vector measured per unit area in the undeformed configuration, $\mathbf{N}$ is an outward unit normal to the surface of the elliptic void in the reference configuration and the steady state nominal axial strain rate equals v_0/L. Because of the assumption of locally adiabatic deformations, no boundary conditions are needed for the thermal problem.

2.1.1. Plate with a through-the-thickness circular thermal defect

The afore-stated problem for the square PC plate is also studied when instead of the elliptic void, there is a circular through-the-thickness region centered at the plate centroid of temperature θ^{def} higher than that of the rest of the body. It will help decipher the effect of the type of defect on the localization of deformation. The problem formulation is identical to that given above except that boundary condition (5g) is ignored and the initial temperature distribution is taken as non-uniform with temperature equal to θ^{def} in the circular cylindrical region and 300 K in the rest of the plate. The temperature of material points at the interface between the defect and the remaining plate is that of the defect where the normal component of the heat flux is taken to be continuous.

2.2. Plane strain simple shearing deformations of a plate

A PC plate of length/height=7, schematically shown in Figure 3, with a thermal defect at its centroid is deformed by equal and opposite tangential velocities prescribed at its top and bottom surfaces such that the nominal steady state strain rate equals 5000/s. To enforce plane strain condition, the out-of-plane displacement of the plate particles is set equal to zero, i.e., x_3-$X_3=0$. The tangential velocity of points on the top and the bottom surface increases linearly from zero to a steady value in time t^0 giving a nominal steady state shear strain rate of v_0/L. The initial temperature of the plate material within the defect is θ^{def} ($\theta^{\text{def}}>300$ K) whereas that of the remaining material is 300 K. The length and the height of the rectangular defect equal 6% of those of the plate that is initially at rest and stress free.

The following boundary conditions are imposed on the plate boundaries:

$$\bar{t}_1=0\ \ \bar{t}_2=0\ \ \text{on}\ X_1=\pm 7L/2 \tag{6a}$$

$$v_1=\begin{cases}\pm v_0\dfrac{t}{t^0}, & 0\le t<t^0\\ \pm v_0, & t\ge t^0\end{cases}\quad v_2=0\quad \text{on}\ X_2=\pm L/2 \tag{6b}$$

Thus, the top and the bottom surfaces of the plate stay flat during deformations and might have normal tractions acting on them.

Equations (1) through (6) are supplemented by constitutive relations reviewed briefly below.

3. Constitutive relations

Referring the reader to [19, 20] for details, we describe essentials of the constitutive relations for the PC. It is assumed that three phases, α, β, and B, co-exist at a material point. At the molecular level, phases α and β correspond to the intermolecular resistance to rotations of main chain segments and of bulky groups, respectively, and phase B to the resistance to chain alignment. In PC, the phase β is due to the resistance to rotation of the phenyl group attached to the main chain [2]. From a continuum mechanics point of view, the phase B accounts for strain hardening and phases α and β for viscoplastic and strain softening effects, respectively. There is neither an explicit yield surface postulated nor the loading/unloading of a material point checked. We use bold face letters to indicate tensorial quantities and affix the subscript i to a quantity to indicate its value for the phase i ($i=\alpha, \beta$, B).

The deformation gradient $\mathbf{F}$ that maps infinitesimal material lines in the undeformed reference configuration to infinitesimal material lines in the present configuration is the same for the three phases and so is the temperature. Similar to the work of Lee [21], the deformation gradient for the α and the β phases is multiplicatively decomposed into elastic and plastic parts, i.e.,

$$\mathbf{F}_{\alpha}=\mathbf{F}_{\alpha}^{\text{e}}\mathbf{F}_{\alpha}^{\text{p}},\ \ \mathbf{F}_{\beta}=\mathbf{F}_{\beta}^{\text{e}}\mathbf{F}_{\beta}^{\text{p}} \tag{7}$$

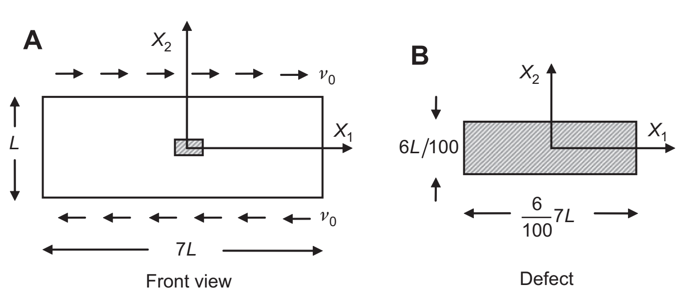

Figure 3 (A) Front view of the plate undergoing plane strain shear deformations and (B) the defect at the centroid of the plate. The origin of the coordinate axes is at the plate centroid.

The plastic deformation gradients $\mathbf{F}_\alpha^{p}$ and $\mathbf{F}_\beta^{p}$ map a material line in a stress-free reference configuration to a material line in the stress-free configuration obtained by elastically unloading the deformed state of the body. Neither $\mathbf{F}^{e}$ nor $\mathbf{F}^{p}$ are gradients of a vector field but $\mathbf{F}$ is the gradient of $\mathbf{x}(\mathbf{X},t)$ with respect to $\mathbf{X}$.

The rate of the plastic deformation gradient in phases α and β is given by:

$$\dot{\mathbf{F}}_\alpha^{p}=\mathbf{F}_\alpha^{e^{-1}}\tilde{\mathbf{D}}_\alpha^{p}\mathbf{F}_\alpha,\quad \dot{\mathbf{F}}_\beta^{p}=\mathbf{F}_\beta^{e^{-1}}\tilde{\mathbf{D}}_\beta^{p}\mathbf{F}_\beta \tag{8}$$

where $\tilde{\mathbf{D}}_i^{p}$ is the plastic strain rate tensor in phase i. The elastic deformation gradient in phase i can be determined from Eq. (7) if the total deformation gradient and the plastic deformation gradient in phase i are known. It has been tacitly assumed in Eq. (8) that the plastic spin tensor in phases α and β identically vanishes.

The plastic strain rate tensor in phase i is assumed to be coaxial with the deviatoric Cauchy stress tensor in phase i, i.e.,

$$\tilde{\mathbf{D}}_\alpha^{p}=\dot{\gamma}_\alpha^{p}\frac{\boldsymbol{\sigma}_\alpha^{'}}{\left|\boldsymbol{\sigma}_\alpha^{'}\right|},\quad \tilde{\mathbf{D}}_\beta^{p}=\dot{\gamma}_\beta^{p}\frac{\boldsymbol{\sigma}_\beta^{'}}{\left|\boldsymbol{\sigma}_\beta^{'}\right|} \tag{9}$$

where $\boldsymbol{\sigma}_i^{'}$ $(i=\alpha,\beta)$ is the deviatoric part of the Cauchy stress $\boldsymbol{\sigma}_i$ in phase i, $\left|\boldsymbol{\sigma}_i^{'}\right|=\sqrt{\mathrm{tr}\left(\boldsymbol{\sigma}_i'\boldsymbol{\sigma}_i'\right)}$ is the magnitude of $\boldsymbol{\sigma}_i^{'}$, tr( ) is the trace operator, and $\dot{\gamma}_i^{p}$ is the effective plastic strain rate in phase i. Eq. (9) implies that tr $(\tilde{\mathbf{D}}_i^{p})=0$, and the plastic strain rate tensors in phases α and β are determined by the deviatoric components of the Cauchy stresses in phases α and β.

The true strain tensor $\boldsymbol{\varepsilon}$ and its magnitude, ε_{mag}, are defined as:

$$\boldsymbol{\varepsilon}=\ln\ \mathbf{V},\quad \mathbf{V}=\left(\mathbf{F}\mathbf{F}^{T}\right)^{1/2} \tag{10}$$

$$\varepsilon_{mag}=\sqrt{\varepsilon_{ij}\varepsilon_{ij}},\quad i,j=1,2,3;\ i \text{ and } j \text{ summed} \tag{11}$$

Thus $\boldsymbol{\varepsilon}$ is the logarithmic strain tensor.

The Cauchy stresses in the α and the β phases are related to their elastic deformations by:

$$\boldsymbol{\sigma}_i=\frac{1}{J_i}\left[2\mu_i\ln\mathbf{V}_i^{e}+\lambda_i\mathrm{tr}(\ln\mathbf{V}_i^{e})\boldsymbol{\delta}\right],\quad i=\alpha,\beta \tag{12}$$

where $J_i=\det(\mathbf{F}_i^{e})$ gives the volume change due to elastic deformations in phase i. In Eq. (12) $\mathbf{V}_i^{e}$ is the logarithmic elastic strain in phase i; $\boldsymbol{\delta}$ is the identity tensor and $\mathbf{V}_i^{e}$ is the left stretch tensor in the polar decomposition of the deformation gradient $\mathbf{F}_i^{e}$ The material elasticities λ_i and μ_i (Lame's constants for infinitesimal deformations) are functions of the current temperature and the present strain rate and capture the temperature-dependent viscoelastic response of the material. As pointed out in [22] the constitutive relation (12) is valid for finite elastic deformations of the body and accounts for all geometric nonlinearities.

The Cauchy stress $\boldsymbol{\sigma}_B$ in phase B is assumed to be deviatoric, and given by:

$$\boldsymbol{\sigma}_B=\frac{C_R}{3}\frac{\sqrt{N_l}}{\lambda^{p}}L^{-1}\left(\frac{\lambda^{p}}{\sqrt{N_l}}\right)\bar{\mathbf{B}}_B' \tag{13}$$

where $\lambda^{p}=\sqrt{\mathrm{tr}\left(\bar{\mathbf{B}}_B\right)/3}$ is a measure of stretch; L is the Langevin function defined by $L(\beta)\equiv\coth\beta-1/\beta$; $\bar{\mathbf{B}}_B'$ is the deviatoric part of $\bar{\mathbf{B}}_B=(\det\mathbf{F})^{-2/3}\mathbf{F}\mathbf{F}^{T}$ and equals $\bar{\mathbf{B}}_B-[\mathrm{tr}(\bar{\mathbf{B}}_B)/3]\ \boldsymbol{\delta}$; N_l is the limiting stretch; $C_R\equiv n_R k\theta$ is the rubbery modulus, θ is the temperature in Kelvin, k is Boltzmann's constant and n_R is a material parameter. The magnitude of the stress in phase B increases exponentially as λ^{p} approaches $\sqrt{N_l}$. For $y=L(x)$, $x=L^{-1}(y)$. Thus the evaluation of $L^{-1}\left(\lambda^{p}/\sqrt{N_l}\right)$ involves solving iteratively a nonlinear equation. The magnitude, σ_{mag}, of the Cauchy stress tensor is defined in the same way as that of the strain tensor; see Eq. (11).

The total Cauchy stress at a spatial point is assumed to equal the sum of the Cauchy stresses in individual phases at that point, i.e.,

$$\boldsymbol{\sigma}=\boldsymbol{\sigma}_\alpha+\boldsymbol{\sigma}_\beta+\boldsymbol{\sigma}_B \tag{14}$$

The effective plastic strain rates in α and β phases are taken to be given by:

$$\dot{\gamma}_i^{p}=\dot{\gamma}_{0i}^{p}\exp\left[-\frac{\Delta G_i}{k\theta}\left(1-\frac{\tau_i}{t_i\hat{s}_i+\alpha_i^{p}p}\right)\right]\quad i=\alpha,\beta \tag{15}$$

Here $\dot{\gamma}_{0i}^{p}$ $(i=\alpha,\beta)$ is the pre-exponential factor, ΔG_i the activation energy, $p=-\sigma_{ii}/3$ the pressure, $\tau_i=\sqrt{0.5\mathrm{tr}\left(\boldsymbol{\sigma}_i^{'}\boldsymbol{\sigma}_i^{'}\right)}$ the effective stress, α_i^{p} the pressure coefficient, $\hat{s}_i=0.077\mu_i/(1-\nu_i)$ the athermal shear strength, ν_i Poisson's ratio, k Boltzmann's constant and t_i an internal variable that evolves with plastic deformations. Eq. (15) gives the pressure, the strain rate, and the temperature dependent evolution of the plastic strain rate in phase i. The variable $\hat{s}_i$ depends upon the temperature because of the dependence of μ_i and ν_i upon the temperature. Because there is no yield surface postulated, plastic deformations always occur. Henceforth we call the maximum magnitude, σ_{mag}, of the Cauchy stress tensor reached before the onset of material softening as the yield stress of the material.

The internal variable t_i equals the athermal shear strength of phase i $(i=\alpha,\beta)$ and its evolution is given by:

$$\dot{t}_i=\frac{h_i}{\hat{s}_i^{0}}\left(1-\frac{t_i}{t_i^{ss}}\right)\dot{\gamma}_i^{p}\quad i=\alpha,\beta \tag{16}$$

where t_i^{ss} and h_i are softening parameters, and $\hat{s}_i^{0}$ is the reference value of $\hat{s}_i$ given by the reference values of μ_i and υ_i. Eq. (16) implies that $\dot{t}_i$ is almost zero when either $\dot{\gamma}_i^{p}$ is close to zero or when t_i is close to t_i^{ss}. Hence, the internal variable t_i remains constant during elastic deformations, and evolves during continued plastic deformations to t_i^{ss}. The strain softening in PCs is captured by the evolution of t_i from an initial value of 1.0 to the final value of t_i^{ss}. Because $\dot{\gamma}_i^p$ depends upon t_i, the right hand side of Eq. (16) is a nonlinear function of t_i and the stress state in phase i.

We postulate that:

$$\dot{Q}=J_\alpha \mathbf{tr}\left(\boldsymbol{\sigma}_\alpha \tilde{\mathbf{D}}_\alpha^p\right)+J_\beta \mathbf{tr}\left(\boldsymbol{\sigma}_\beta \tilde{\mathbf{D}}_\beta^p\right) \tag{17}$$

Thus the energy dissipated due to plastic working equals the sum of energies dissipated due to plastic working in phases α and β. Moreover, all of the plastic working is assumed to be converted into heating giving the Taylor-Quinney factor equal to 1.

3.1. Values of material parameters

Values of material parameters for the PC tested by Mulliken and Boyce [2] are listed in Table 1. Consistent with their assumption that deformations of phase β are affected only by positive pressures, we set the pressure coefficient α_β^p equal to zero if the pressure is negative. The elastic parameters λ_i and μ_i ($i=\alpha,\beta$) are given by:

$$\lambda_i=\frac{E_i(1+\nu_i)}{2},\quad \mu_i=\frac{E_i}{2(1+\nu_i)} \tag{18}$$

Here E_i and ν_i are Young's modulus and Poisson's ratio for phase i, respectively. Values of E_α and E_β as functions of the temperature and the strain rate(s) are not listed in Table 1 because they are derived from functions given as MATLAB routines in Appendices C and D of Mulliken's thesis [23], which were converted to FORTRAN® 90 subroutines. Values of E_α and E_β at 300 K and the nominal strain rate of 5000/s equal, respectively, 1.678 GPa and 0.345 GPa for the PC.

The simulation of simple tensile deformations of a body comprised of phase α revealed that a change in the value of the internal variable t_α from 0.9 to 0.6 increased the value of $\dot{\gamma}_\alpha^p$ by an unrealistic 13 orders of magnitude. Accordingly, Eq. (15) is modified to:

Table 1 Values of material parameters for the modified constitutive equations for the PC; for values of Young's modulus study the paragraph following Eq. (18).

	Phase α	Phase β	Phase B
ν_i	0.38	0.38	
$\dot{\gamma}_{0i}^p$ (/s)	2.94×10^{16}	3.39×10^5	
ΔG_i (J)	3.744×10^{-18}	3.769×10^{-20}	
α_i^p	0.168	0.245	
h_i (MPa)	125	400	
t_i^{ss}	0.33	2.00	
C_R at 300 K (MPa)			35.0
N_l			12.25
c [J/(gm-K)]	1.20		
ρ (kg/m³)	1.20		

$$\dot{\gamma}_i^p=\min\left(\dot{\gamma}_{0i}^p \exp\left[-\frac{\Delta G_i}{k\theta}\left(1-\frac{\tau_i}{t_i\hat{s}_i+\alpha_i^p p}\right)\right], 10^5\,/\mathrm{s}\right),\quad i=\alpha,\beta \tag{19}$$

that limits the maximum effective plastic strain rate in phases α and β to 10^5/s.

We note that for the PC, $\dot{\gamma}_{0\alpha}^p$ and $\dot{\gamma}_{0\beta}^p$ are of the order of 10^{16} and 10^5, respectively.

4. Strain localization criterion

We hypothesize that deformations in a PC begin to localize at a material point when the magnitude of the true strain tensor given by Eq. (10) equals at least twice the nominal strain and either $\dot{\gamma}_\alpha^p$ or $\dot{\gamma}_\beta^p$, or both equal at least twice the applied nominal strain rate. For each of the problems studied, the steady state nominal strain equals $\nu_0 t/L$. Results presented below do depend upon the strain localization criterion; however, our extensive work (e.g., see [24, 29]) with metals suggests that results using different localization criteria are qualitatively similar but might vary quantitatively.

In experiments, it is rather difficult to decipher when precisely the deformation begins to localize. One could potentially use the digital image correlation technique to find out when the localization process starts on the outer surface of a body and also compute the strain rate within the zone of localized deformation. Measurements on the bounding surface of a body provide very little information about the state of deformation in the interior of the body for large deformations.

5. Numerical solution of the governing equations

The IBV problem is solved using the commercial FE software, LS-DYNA (www.lstc.com), in which the constitutive equations are implemented as a user defined subroutine. We used eight-node brick elements with eight-point integration rule and a lumped mass matrix derived from the consistent mass matrix by the row sum technique. Equations of motion are integrated with an explicit conditionally stable algorithm and the time step size is taken as a fraction of that required for the elastic dilatational wave to propagate through the smallest element in the mesh. The unknowns at an integration point are $\mathbf{x}$, $\mathbf{v}$, $\mathbf{F}_\alpha^p$, $\mathbf{F}_\beta^p$, t_α, t_β, θ and the mass density ρ. For a 3D problem, the number of unknowns at a node equals 28. The verification of the user defined subroutine for isothermal deformations is described in [19].

5.1. Results for the plate with an elliptical void

Referring to Figure 2, we set $h=0.04$ mm, $L=1$ mm, $\nu_0=$ 5 m/s and $t^0=1$ μs, giving the steady state nominal axial strain rate equal to 5000/s. For results discussed in subsections 5.1.1–5.1.8, we take $a=b=0.04$ mm. We have selected small dimensions of the specimen so that we can ascertain the width of the region (expected to be in micrometers) of the localized deformation within reasonable computational resources.

5.1.1. Effect of the FE mesh Using the mesh generator add-on in Tecplot 360 (www.tecplot.com), the half-thickness of the plate is divided into five uniform layers and the FE meshes for two voids on the plane X_3=constant for a/b=1, 1/4 are shown in Figure 4. The total number of elements (nodes) for each case equaled 20,000 (24,846) with the boundary of the ellipse in the first quadrant discretized into 40 straight line segments of equal length. For each void, the principal axes of the ellipse coincided with the X_1- and the X_2-axes and the major axes measured 0.08 mm. Thus for a/b=4, the major axes is aligned with the X_2-axis and for a/b =1/4 with the X_1-axis.

In order to get an idea of the error in the numerical solution, we analyzed deformations of the PC plate using the two meshes described below; the finer mesh is referred to as mesh 2. In the two discretizations near the elliptic void shown in Figure 5, the number of elements along the boundary of the ellipse, near the elliptic void, and in the thickness direction was increased by 50% in mesh 2 as compared to those for mesh 1 resulting in 20,500 (19,800) and 47,040 (39,984) nodes (elements), respectively, in meshes 1 and 2.

Three points within the narrow region of intense deformations and their coordinates in the reference configuration for the two meshes are exhibited in Figure 6. For a node in mesh 1, the node closest to that node in mesh 2 was chosen to compare the results because nodes in the two meshes do not coincide with each other. Because a narrow region of severe deformations had formed in the plate at 25 μs, we show in Figure 7 time histories of σ_{mag} and ε_{mag} at these points until t=25 μs. Over the duration of the simulations, the maximum difference in σ_{mag} and ε_{mag} from results with

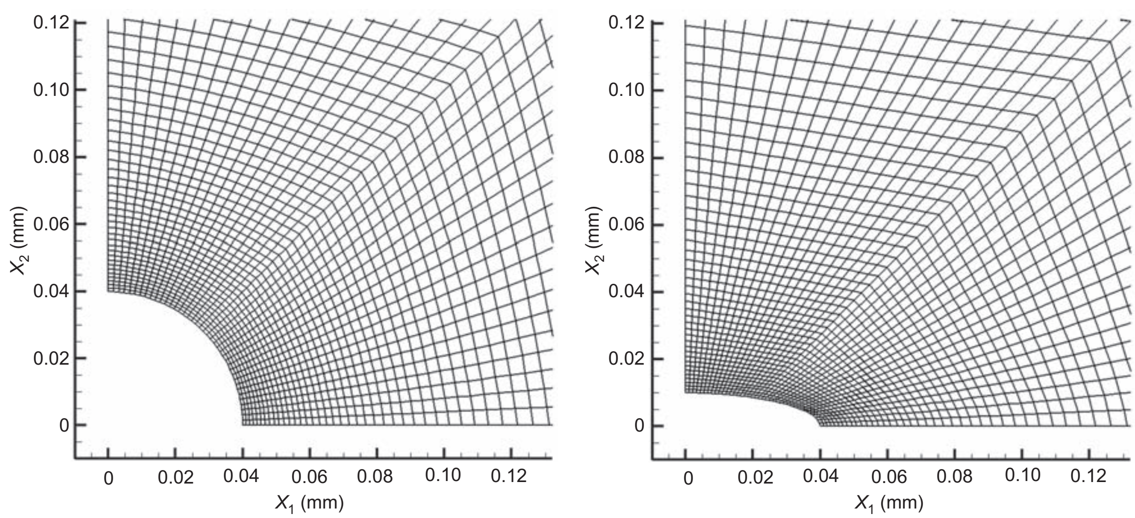

Figure 4 Discretization of the plate on the plane X_3=0 near the through-the-thickness elliptic void for a/b=1 (left) and a/b=1/4 (right).

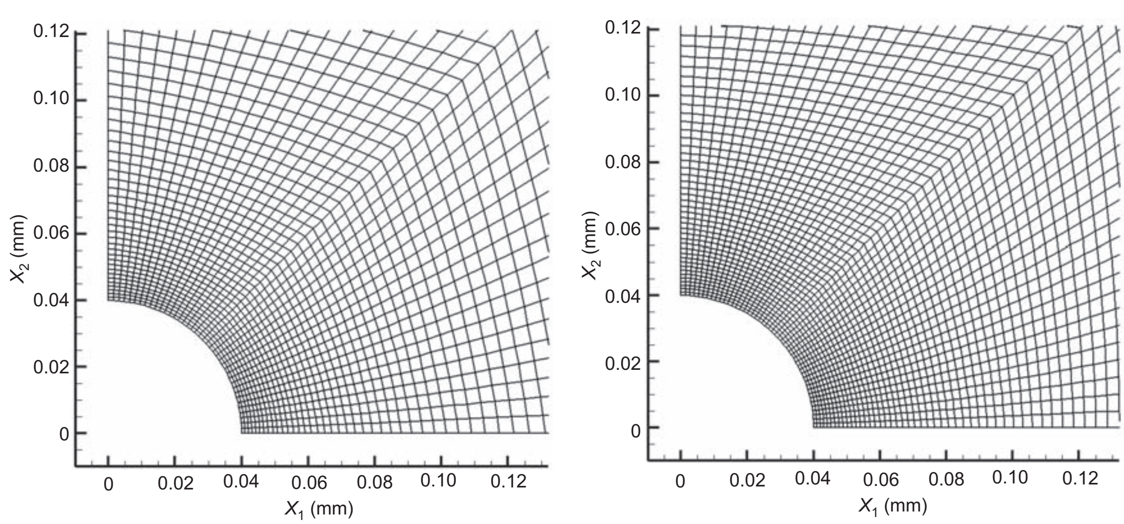

Figure 5 Discretization of the plate near the void on the plane X_3=0 for mesh 1 (left) and mesh 2 (right).

the two meshes at any one of the three points considered was 9%. Results presented below computed with mesh 1 provide a good qualitative description of the localization of deformation and if desired the quantitative information can be improved upon by computing results with successively finer meshes.

5.1.2. Localization of deformation At time $t=26$ µs, contour plots of ε_{mag} on the front face $X_3=0.02$ mm and in a small region near the circular void on the plane $X_2=0$ are exhibited in Figure 8. It can be seen that a band of intense strain has developed in the plate with the strain near the void tip exceeding 1.0. The value of ε_{mag} reaches 1.0 first at the tip (0.04, 0, 0) of the circular void on the X_1-axis and is in the mid-surface of the plate. The effective strain is essentially uniform through the plate thickness at least near the void surface. If we define the width of the band as the thickness of the region in which ε_{mag} equals about 0.5, then we get ~18 µm as the band width.

Figure 9 exhibits the time history of ε_{mag} and the temperature at two points (0.04, 0, 0) and (0.04, 0, 0.02), where the strain localization condition is satisfied at 3.12 µs and 4.50 µs, respectively. At each one of the two points, the temperature increases monotonically until it equals ~380 K at ~17 µs and

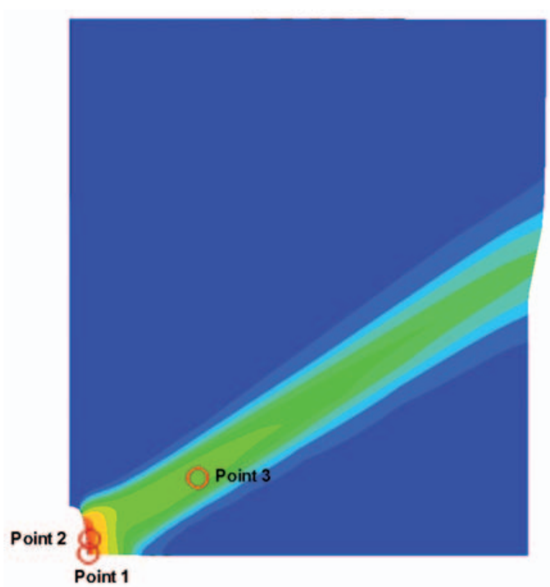

MESH–1	X_1	X_2	X_3
Point 1	0.040	0.000	0.02
Point 2	0.049	0.012	0.02
Point 3	0.292	0.129	0.02
MESH–2	X_1	X_2	X_3
Point 1	0.040	0.000	0.02
Point 2	0.048	0.011	0.02
Point 3	0.289	0.128	0.02

Figure 6 Locations of three points considered for comparing results from the two FE meshes (left) and their coordinates, in mm (right), in the reference configuration.

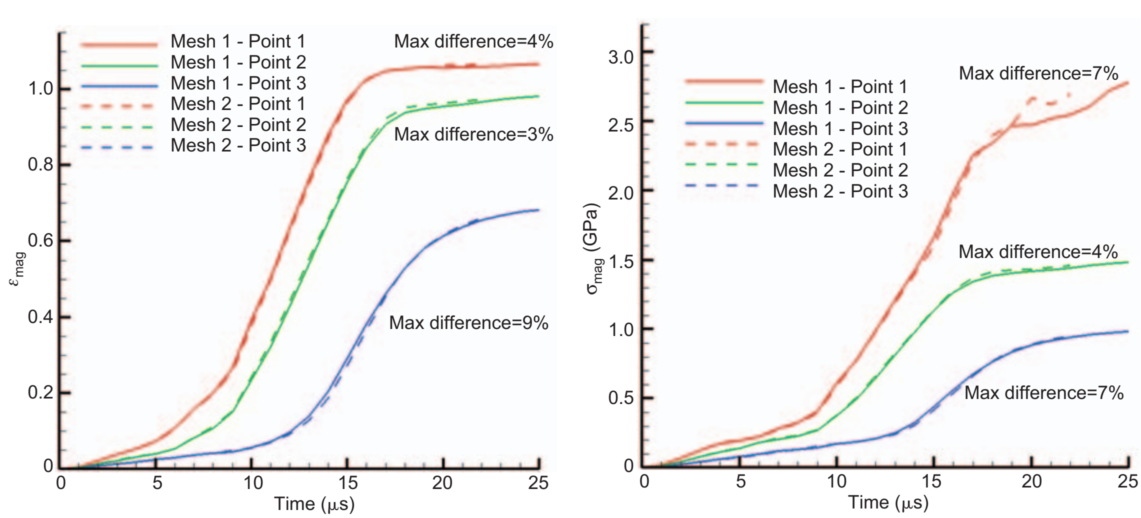

Figure 7 Time histories of ε_{mag} (left) and of σ_{mag} (right) at the three points in the plate from the two FE meshes.

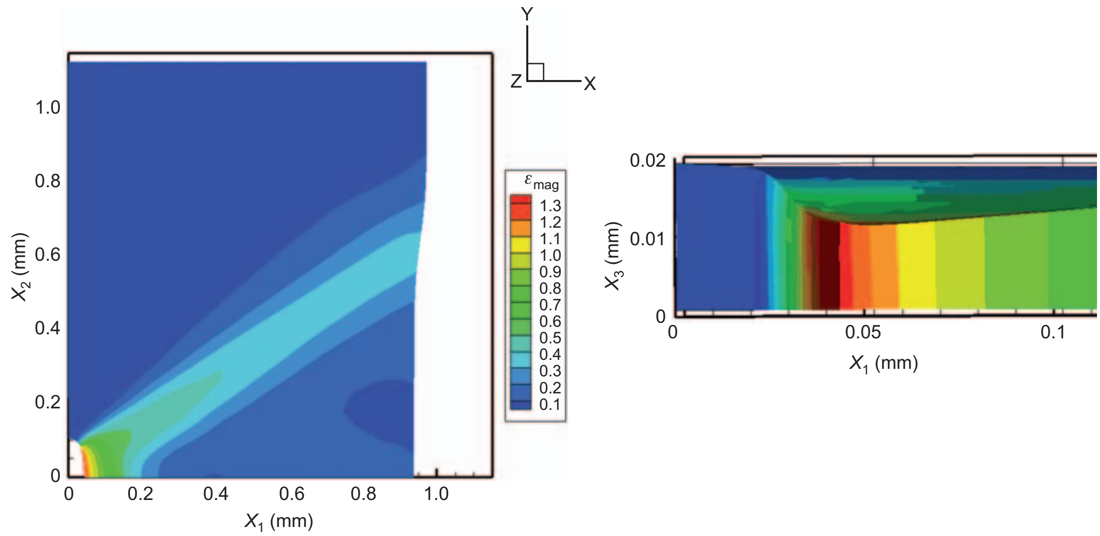

Figure 8 At $t=26$ μs contour plots of ε_{mag} on the surface $X_3=0.02$ mm (left) and near the void on the plane $X_2=0$ (right).

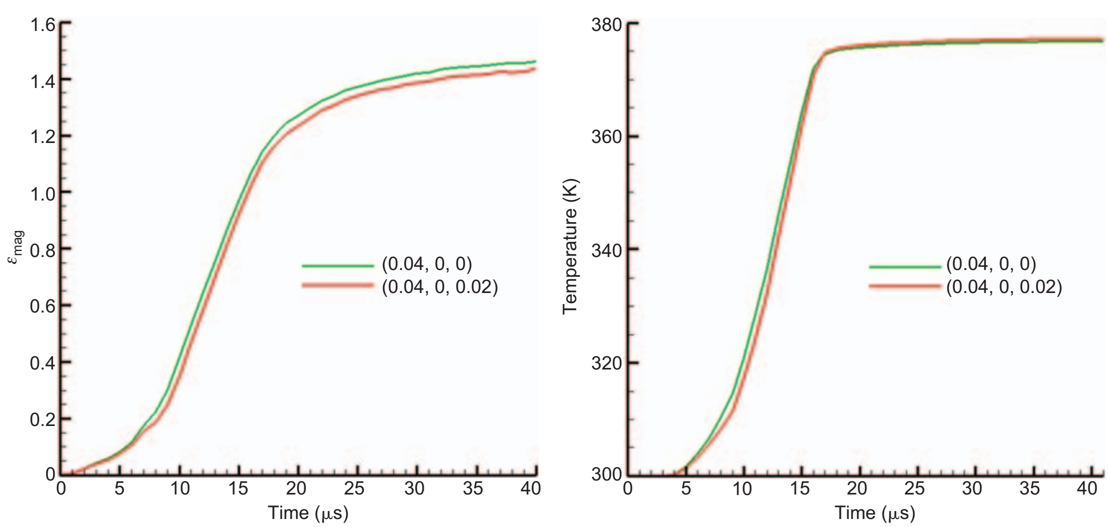

Figure 9 Time histories of ε_{mag} (left) and of the temperature (right) at points (0.04, 0, 0.02) and (0.04, 0, 0).

stays there subsequently because the average plastic strain-rate and hence the plastic working become null. For a typical PC, the yield stress of the material drops noticeably at $\theta=380$ K; e.g., see Figure 1 in Bauwens-Crowet et al. [25]. The maximum strain rate at both points equals ~10^5/s; values of $\dot{\varepsilon}_{mag}$ are found by differentiating ε_{mag} with respect to time t by the backward difference method.

5.1.3. Strain localization band From fringe plots of shear strains ε_{12}, ε_{13} and ε_{23} near the void and over the entire domain on the front face $X_3=0.02$ mm of the plate at $t=26$ μs depicted in Figure 10, it can be seen that the maximum magnitudes of ε_{12}, ε_{13}, and ε_{23} equal ~0.41, ~0.18 and ~0.11, respectively, which are less than one-half of the maximum value of ε_{mag} (Figure 8). Also, magnitudes of shear strains over most of the domain are close to zero and the high shear strains are concentrated in a small region near the void and none of the three fringe plots show a band of high shear strain.

Figure 11 shows fringe plots of principal stretches (eigenvalues of the left or the right stretch tensor) at $t=26$ μs on the deformed shape of the plane $X_3=0.02$ mm. The overall elongation of the plate equals about 12% and its maximum contraction ~8%. Recalling that a stretch equals 1.0 in the reference configuration, a line element near the void surface and close to the horizontal plane $X_2=0$ is stretched by ~230% and another one in the same general location contracted by ~40%. Thus the normal strains in the narrow region of localized deformation are much higher than the shear strains. The eigenvectors for the maximum principal stretch lie in the plane $X_3=$constant and are parallel to the boundary of

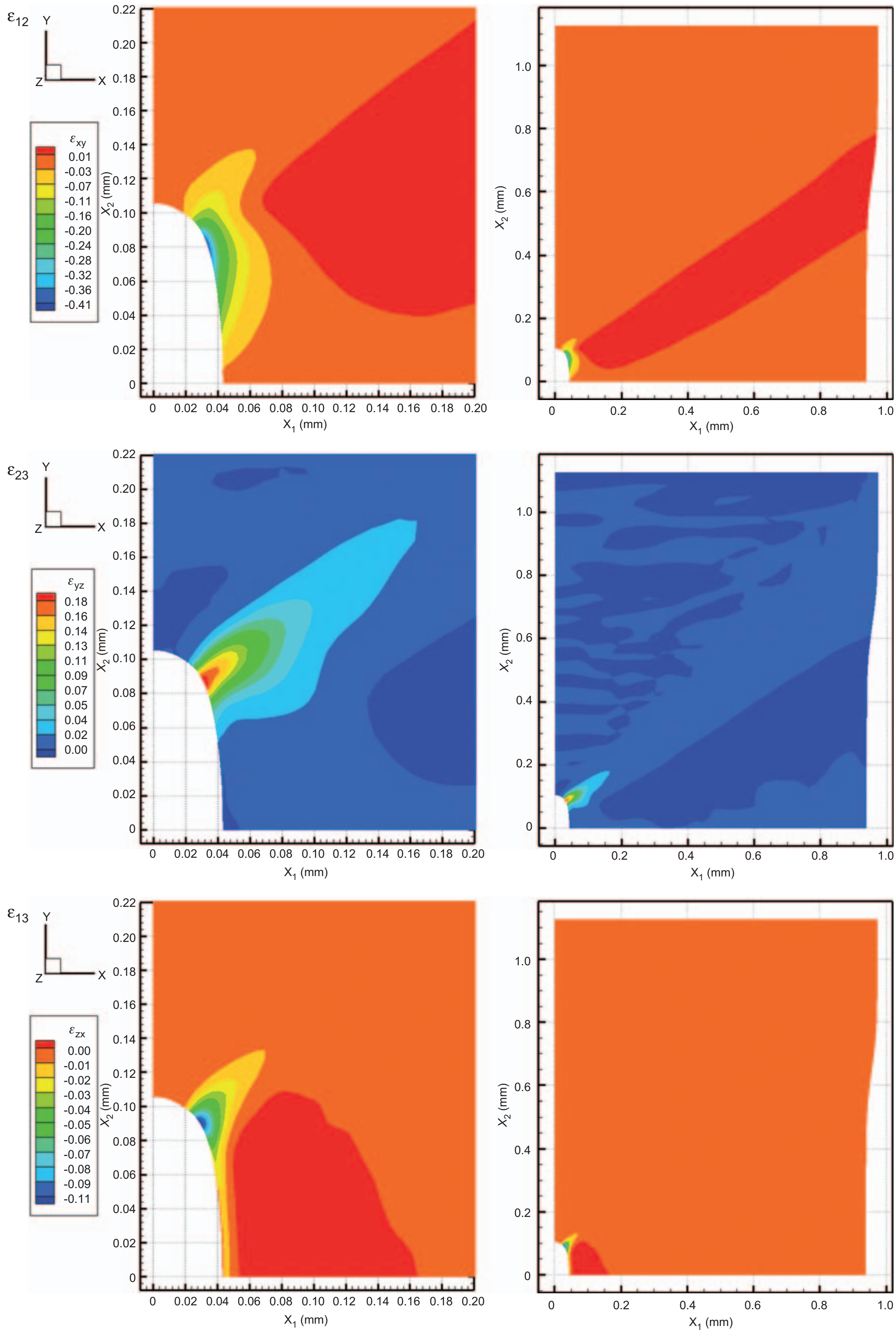

Figure 10 Fringe plots of ε_{12}, ε_{23} and ε_{13} at $t=26$ μs near the void (left) and over the entire domain (right) on the plane $X_3=0.02$ mm.

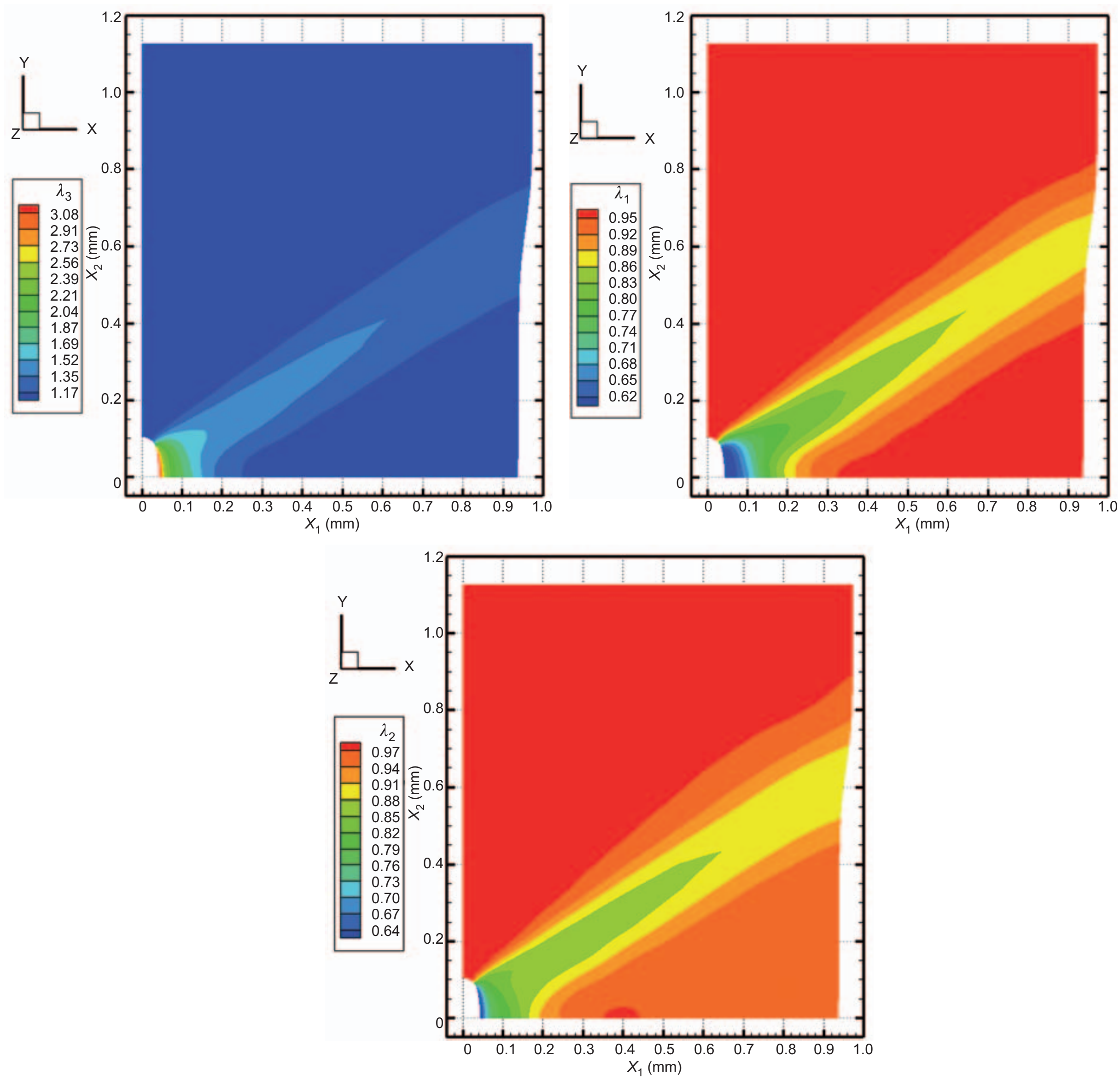

Figure 11 At $t=26$ μs fringe plots of the three eigenvalues of the left or the right stretch tensor on the deformed shape of the front face $X_3=0.02$ mm of the plate.

the geometric defect. The X_3-axis is the eigenvector for one of the other two principal stretches and the eigenvector for the 3rd principal stretch is along the normal to the boundary of the geometric defect. Eigenvectors of the left stretch tensor give directions of principal stretches in the deformed configuration.

Whereas for the present problem, the principal stretches are much larger than the maximum shear strains within the band of localized deformation, Lu and Ravi-Chandar [11], and Wu and van der Giessen [15] found the maximum shear strain within the band to be dominant during simple tensile and plane strain simple shearing deformations of a PC body. Lu and Ravi-Chandar approximated the material response by a trilinear axial stress – axial strain curve, and Wu and van der Giessen used constitutive relations similar to those employed here except that they assumed strain rates to be very small, neglected inertia forces and introduced a weak region with a smaller value of the yield stress to trigger the initiation of localization of deformation.

5.1.4. Propagation of the band of intense deformations Figure 12 depicts fringe plots of $\dot{\varepsilon}_{mag}$ on the deformed shape of the plate's front face $X_3=0.02$ mm at $t=14$, 24 and 34 μs; the legend indicates strain rates in 10^6/s thus the maximum strain rate at a point within the region of localization is ~10^5/s. At 14 μs, the region of the high true strain rate emanating from the void periphery is simply connected, which at 24 μs widened and the point of

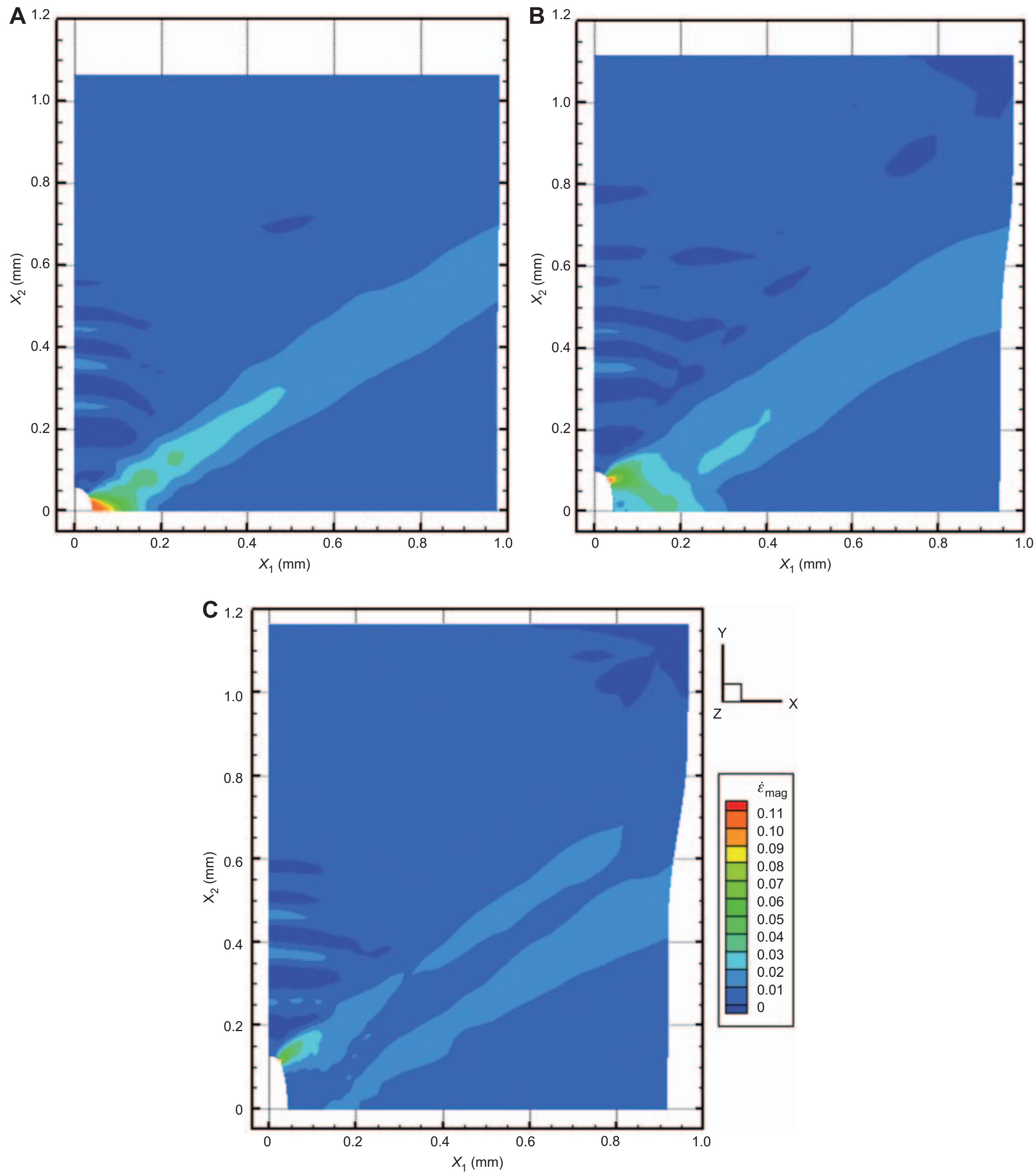

Figure 12 Fringe plots of the maximum $\dot{\varepsilon}_{mag}$ on the deformed shape of plate's front face $X_3=0.02$ mm at $t=14$ μs (A), $t=24$ μs (B), and $t=34$ μs (C).

maximum $\dot{\varepsilon}_{mag}$ moved along the boundary of the void. The simply connected region split into two disconnected regions of high $\dot{\varepsilon}_{mag}$ at $t=34$ μs. Also, points of high value of $\dot{\varepsilon}_{mag}$ at 14 μs become points of low value of $\dot{\varepsilon}_{mag}$ at 24 μs and later. This splitting of the narrow region of high strain rate into two parts has not been reported by previous investigators [11, 15]. Note that at each one of the three times, there are small regions away from the void where the strain rate varies between 10^3/s and 10^4/s.

The high value of $\dot{\varepsilon}_{mag}$ at a point causes the deformation to increase rapidly, the stress in phase B increases exponentially with an increase in $\lambda^p/\sqrt{N_l}$, the material hardening in phase B overcomes material softening in the α and β phases and the deformation stabilizes. The drop in the value of $\dot{\varepsilon}_{mag}$ at a material point is attributed to its strain hardening. This can be seen from the fringe plots of $\lambda^p/\sqrt{N_l}$ near the void on the plane $X_3=0.02$ mm at $t=14$, 24, and 34 μs given in Figure 13.

Recalling that λ^p depends upon the deformation gradient, the value of $\lambda^p/\sqrt{N_l}$ increases from 0.286 at t=0 as a material point deforms. At $t=14$ μs, the hardening in the material is confined to a small region near the tip of the void, but at $t=24$ μs, $\lambda^p/\sqrt{N_l}$ increases by 80% at points close to the circular void and the true strain rate at those points decreases by a factor of three. On further deformation the material within the band hardens, the band widens and the region of high values of $\dot{\varepsilon}_{mag}$ has the hardened material.

The interaction between the softening and the hardening at a material point is further illustrated in the time history plot, presented in Figure 14, of effective stresses in the α and β phases, and of $\dot{\varepsilon}_{mag}$ at the point (0.04, 0, 0.02). Until t=10 μs effective stresses in phases α and β increase monotonically; subsequently the effective stress in phase α drops but that in phase β continues to increase monotonically for the time duration, 40 μs, of the computation. Recalling that $\dot{\gamma}^p_{0\alpha}$ and $\dot{\gamma}^p_{0\beta}$ are of the order of 10^{16} and 10^5 respectively, deformations of phase α contribute more to the value of $\dot{\varepsilon}_{mag}$ than those of phase β. For $t>15$ μs, as phase α hardens $\dot{\varepsilon}_{mag}$ begins to decrease because the softening in phase β is not strong enough to overcome the hardening in phase α deformations of the material point stabilize and $\dot{\varepsilon}_{mag}$ decreases.

Figure 15 exhibits time histories of ε_{mag} and of the inverse Langevin function at the point (0.04, 0, 0.02). The value of ε_{mag} begins to increase rapidly at ~10 μs, the plateau in the rate of increase of ε_{mag} at ~16 μs coincides with the instant of the rapid increase in the inverse Langevin function and that of the drop in the value of $\dot{\varepsilon}_{mag}$.

5.1.5. Effect of strain rate Deformations of the PC plate were also studied at nominal axial strain rates of 1, 50, 1000,

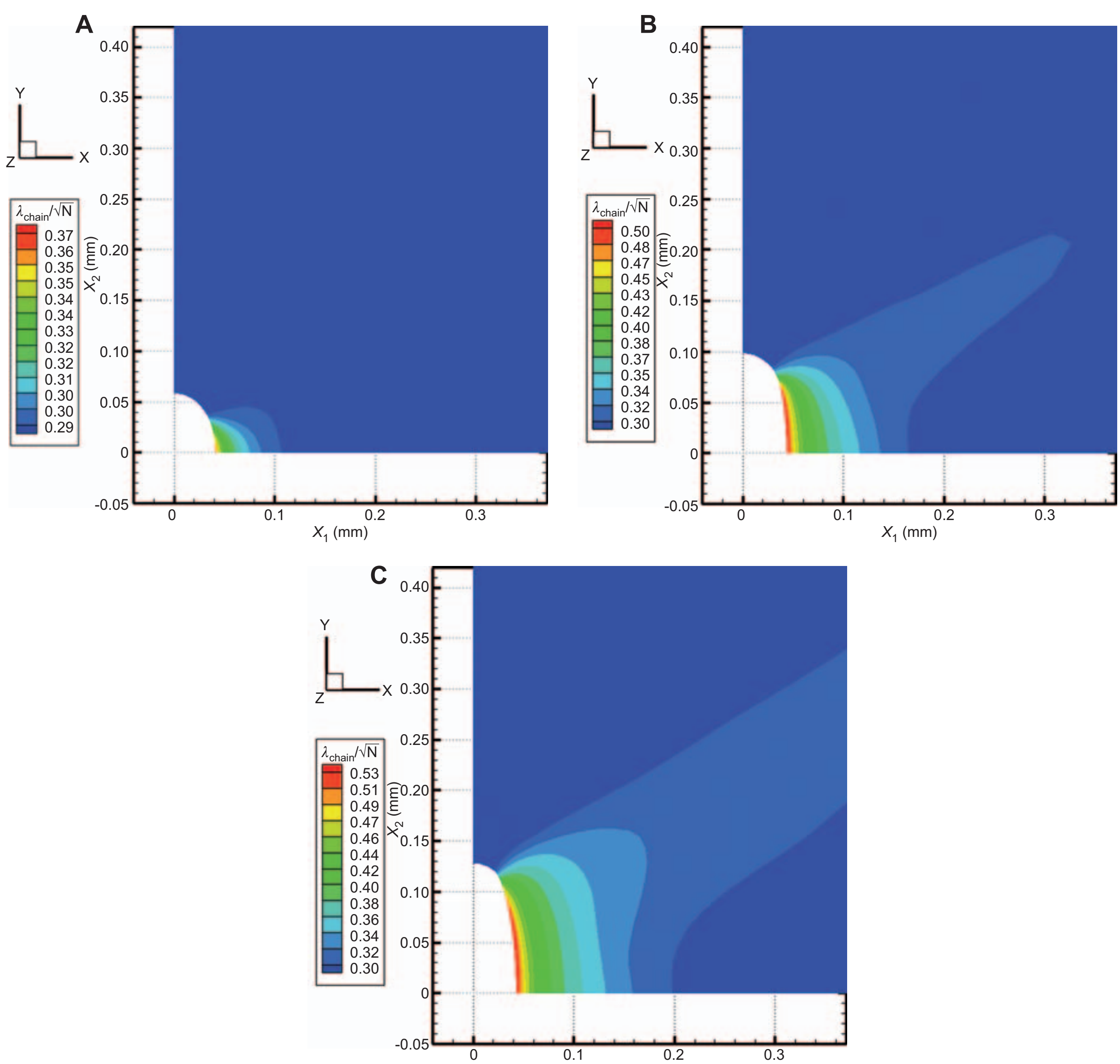

Figure 13 Fringe plots of $\lambda^p/\sqrt{N_l}$ near the void in the reference configuration of the plane $X_3=0.02$ mm at $t=14$ μs (A), $t=24$ μs (B) and $t=34$ μs (C).

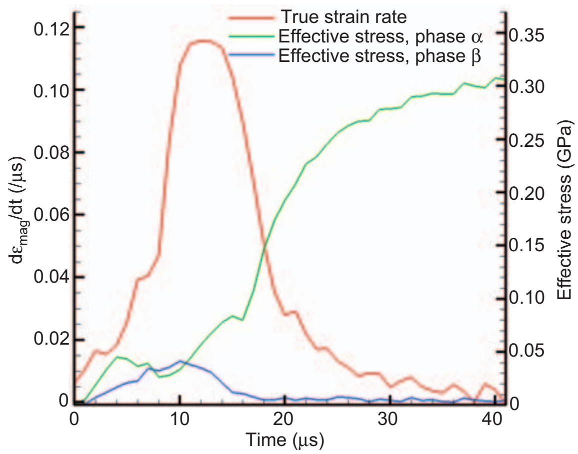

Figure 14 Time histories of the effective stress in phases α and β, and of $\dot{\varepsilon}_{mag}$ at the point (0.04, 0, 0.02).

3000, 7000, and 10,000/s. To decrease the computational time of simulations at nominal strain rates of 1 and 50/s, we increased the mass density of the material by a factor of 10^3 and 10^2, respectively, to use larger time steps for temporal integration than those possible for the normal value of the mass density.

At a strain rate of 1/s, the propagation of localized deformations is different from that at the strain rate of 5000/s described in the previous section. We compare in Figure 16 fringe plots of ε_{mag} near the void for plates deformed at 5000/s on the plane $X_3=0$, and at 1/s on planes $X_3=h/2=0.02$ mm and 0 when the nominal axial strains in the plate were 8, 9 and 10%. At strain rate of 1/s, the localized deformations initially propagated along the X_1-axis but on further deformation propagated along a direction close to that when the strain rate is 5000/s. However, on the plane $X_3=0.02$ mm, the band for the nominal strain rate of 1/s was initially inclined to the X_1-axis. The propagation of localized deformations along the X_1-axis was not observed for the five strain rates higher than

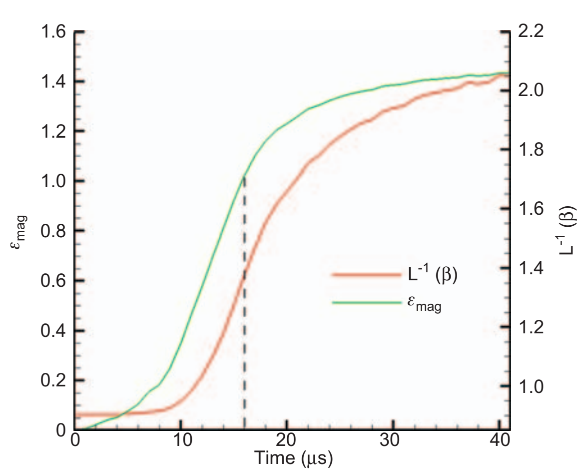

Figure 15 Time histories of ε_{mag}, and of the inverse Langevin function at the point (0.04, 0, 0.02).

1/s considered here. Furthermore, the band of localized deformations for the applied strain rate of 5000/s is nearly three times as wide as that for the applied strain rate of 1/s.

The nominal axial strain when the strain localization condition is first satisfied at the five points along the band marked in Figure 17 and its average speed of propagation in the reference configuration of PC plates deformed at different strain rates are listed in Table 2. The coordinates in the undeformed configuration of the five points are listed in Table 3. At the nominal axial strain rate of 1/s the propagation of the localized deformations did not follow the same path as that at the other strain rates considered here. Hence, at strain rate of 1/s five points were chosen within the band such that they have the same X_1 and X_3 coordinates in the undeformed configuration as the five points in Figure 17, but have different X_2 coordinates that are listed in Table 3. The average speed of propagation is computed by dividing the distance between points 1 and 5 in the undeformed configuration by the difference in the localization times for those two points.

From the data in Table 3, we conclude that the nominal axial strain at the initiation of localization of deformation at a point and the average band speed increase with an increase in the applied nominal axial strain rate.

5.1.6. Effect of pressure-dependent yielding To check the influence of pressure-dependent yielding on the localization phenomenon, we computed deformations of the plate with the pressure coefficients α_α^p and α_β^p in Eq. (19) set equal to the six values listed in Table 4 and the nominal axial strain rate equal to 5000/s. Results of the six simulations were essentially close to each other; a band of high strain was observed in all the simulations and it had high stretches rather than high shear strains. Thus the pressure-dependent yielding is not responsible for the principal stretches rather than the shear strains being large within the region of localized deformation.

The times when the localization condition is satisfied at the five points along the band marked in Figure 17 and the average speed of propagation of the band for the six simulations described above are listed in Table 5. The maximum difference in values of times and the average speed for these six simulations is ~20% implying that values of α^p_α and α^p_β do not affect much either the time when the deformation localizes at a point or the average speed of propagation of the band. Also, the angle between the centerline of the region of the localized deformation and the x_1-axis was nearly the same for these six simulations.

5.1.7. Softening modulus E_s In an attempt to find a material parameter that characterizes whether or not deformations in a PC localize, we introduce the softening modulus, E_s, defined as the minimum slope of σ_{mag} vs. ε_{mag} curve during the strain softening regime. For the σ_{mag} vs. ε_{mag} curve shown in Figure 18, E_s equals the magnitude of the slope of line AC, i.e., it equals AB/BC.

For metals, Wright and Walter [26] among others, hypothesized that E_s determines the propensity of a material

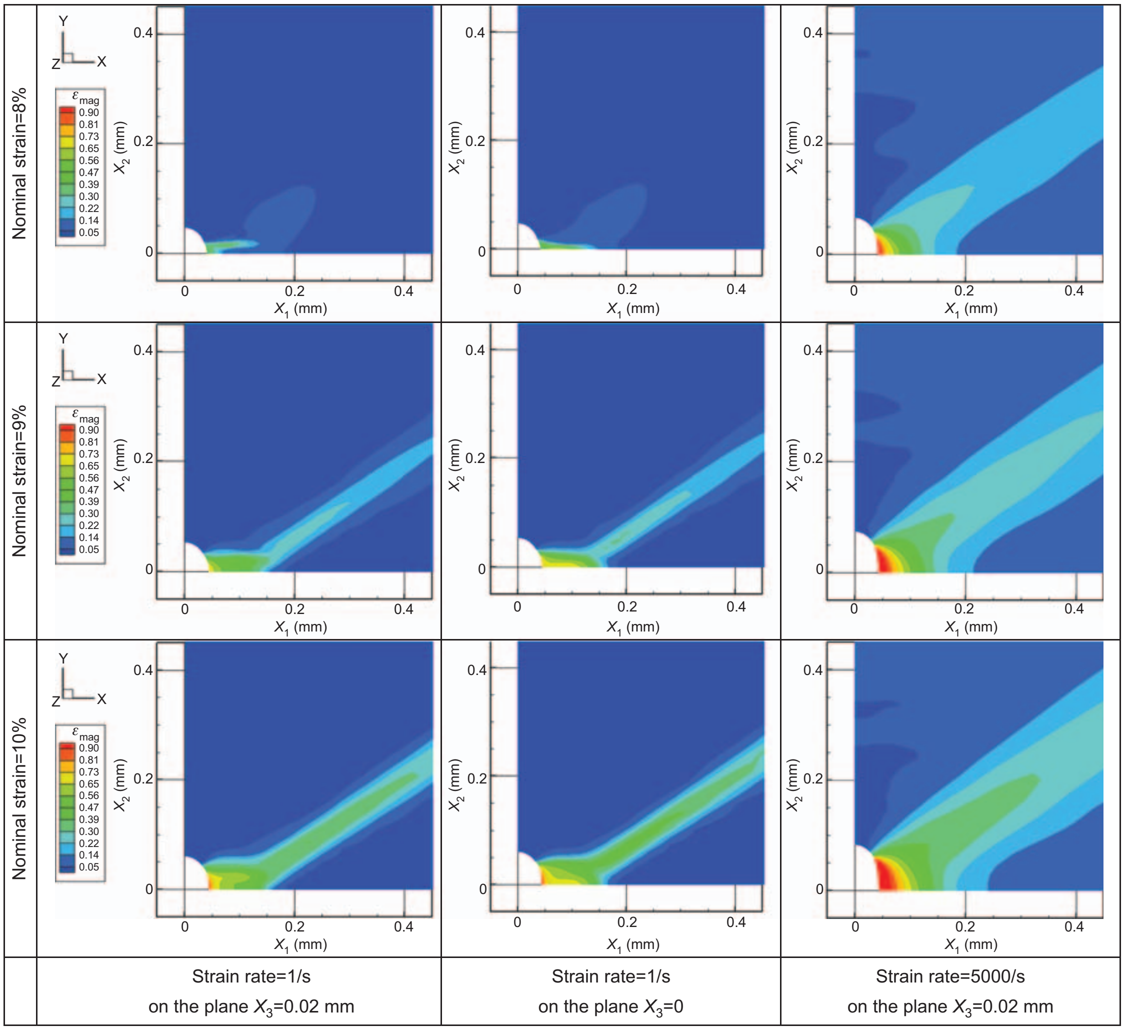

Figure 16 Near the void fringe plots of ε_{mag} for PC plates; (left) on the plane $X_3=0.02$ and nominal axial strain rate = 1/s, (center) on the plane $X_3=0.0$ and nominal axial strain rate = 1/s, (right) on the plane $X_3=0.02$ and nominal axial strain rate = 5000 /s. Values of the nominal axial strain for these fringe plots are listed in the left column.

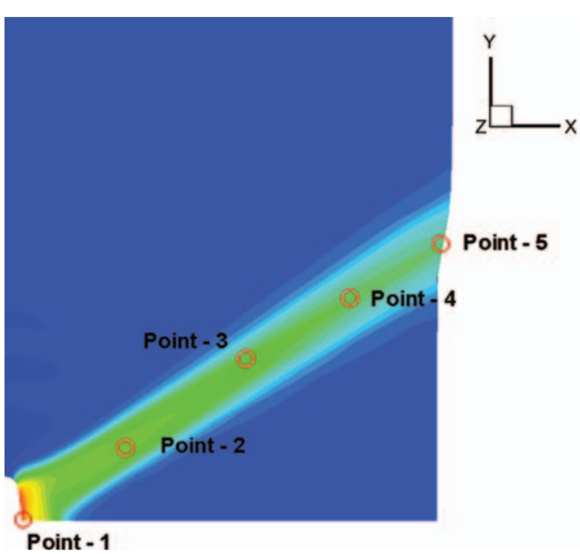

Figure 17 Five points of interest along the strain localized band.

to shear strain localization. The strain softening in the constitutive relations of a PC is governed by Eq. (16) and it depends on values of material parameters h_i and t_i^{ss} ($i=\alpha, \beta$). Here, we study the softening only in phase α because softening in both phases is governed by the same equation with only different values of material parameters. For various values of h_α and t_α^{ss}, the σ_{mag} vs. ε_{mag} curves for uniaxial compressive deformations at a nominal axial strain rate of 5000/s are depicted in Figure 19. Values of E_s computed from these curves and others not shown here are listed in Table 6. These reveal that for the same nominal axial strain rate E_s in tensile deformations generally differs from that in compressive deformations. For both compressive and tensile deformations, the value of E_s decreases with a decrease in h_α and an increase in t_α^{ss}. Furthermore, the value of E_s depends upon the present strain rate, the current temperature and the strain hardening parameters. Hence, the variation of the elastic modulus with the strain rate and the temperature will influence the value of E_s. Note that values

Table 2 Nominal strain in the plate when strain localization initiates at points in Figure 17 and the average speed of propagation of the localized deformations.

Strain rate (/s)	Nominal axial strain at which strain localization initiates (%)					Band speed (m/s)
	Point 1	Point 2	Point 3	Point 4	Point 5	
1	0.14	4.25	4.44	4.60	4.62	0.0247
50	1.16	5.52	6.23	6.77	6.92	0.96
1000	1.62	6.25	7.62	9.36	9.29	14.4
3000	1.81	6.49	8.05	9.13	9.19	45.0
5000	1.82	6.94	8.23	8.61	8.77	72.8
7000	2.14	7.45	8.65	9.55	9.89	100.0
10,000	2.05	7.72	9.67	10.83	11.31	119.5

Table 3 Coordinates of the five points in Figure 17 in the reference configuration.

Point	X_1 (mm) all strain rates	X_2 (mm) strain rate of 1/s	X_2 (mm) strain rate higher than 1/s	X_3 (mm) all strain rates
1	0.04	0.00	0.00	0.00
2	0.29	0.11	0.14	0.00
3	0.56	0.28	0.31	0.00
4	0.81	0.41	0.45	0.00
5	1.00	0.55	0.55	0.00

of h_α and t_α^{ss} listed in Table 6 are for fictitious materials. A negative value of the softening modulus implies that no strain softening is observed for the material.

In Eq. (16), the variation of t_α affects only stresses in phase α but the Cauchy stress at a material point equals the sum of the Cauchy stresses in phases α, β and B. Hence, even though the stress in phase α might decrease, the total stress at a point could increase.

5.1.8. Effect of the softening modulus on plates with circular voids For a PC plate with a through-the-thickness circular void and made of materials with E_s less than or equal to ~75 MPa deformed in tension at a nominal axial strain rate of 5000/s and initial temperature of 300 K, a band of localized deformation did not form in the plate. The localization initiation condition was satisfied at points near the geometric defect but not at points away from the defect. For different values of h_α and t_α^{ss}, we have listed in Table 7 the localization initiation times for the five points within the band (Figure 17). Because of the inhomogeneous deformations of the plate, the effective plastic strain rate and the temperature rise will be different at various points of the plate. Thus the σ_{mag} vs. ε_{mag} curve and the values of E_s will vary from point to point in the plate. The values of h_α and t_α^{ss} are the same for every point of the plate but not necessarily those of E_s unless plate's deformations are homogeneous.

The data in Table 7 is plotted in Figure 20 as the percentage change in the localization initiation time compared to that of the PC (h_α=125 MPa and t_α^{ss}=0.33) vs. the ratio of E_s for the fictitious material to that of the PC. The softening modulus is determined from simulations of uniaxial compression at a nominal axial strain rate of 5000/s and a

Table 4 Values of the pressure coefficient for phases α and β for the six simulations conducted to study the influence of the pressure dependent yielding; the row shaded in grey corresponds to material parameters for the PC.

Simulation number	Pressure coefficient (α_i^p)	
	Phase α	Phase β
1	1.68×10^{-1}	2.45×10^{-1}
2	1.68×10^{-2}	2.45×10^{-2}
3	1.68×10^{-3}	2.45×10^{-3}
4	0.0	0.0
5	0.0	2.45×10^{-1}
6	1.68×10^{-1}	0.0

Table 5 Localization initiation times at the five points along the band and the average speed of propagation of the band for the six simulations with values of α_α^p and α_β^p listed in Table 4; the row shaded in grey corresponds to material parameters for the PC.

Simulation number	Localization initiation time (μs)					Band speed (m/s)
	Point 1	Point 2	Point 3	Point 4	Point 5	
1	4.40	14.31	16.32	17.96	18.68	78
2	4.28	16.21	17.85	20.29	20.70	67
3	5.57	16.49	17.86	19.82	20.63	73
4	5.01	16.56	18.26	20.88	21.56	67
5	4.50	16.35	17.49	19.65	20.42	70
6	5.05	14.39	16.14	17.84	18.54	82

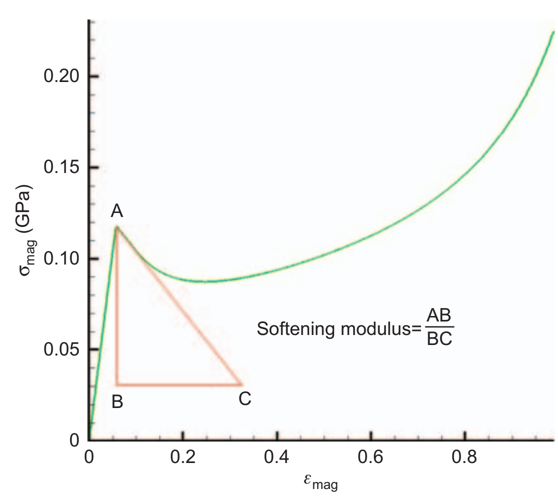

Figure 18 Schematic diagram illustrating the softening modulus, E_s.

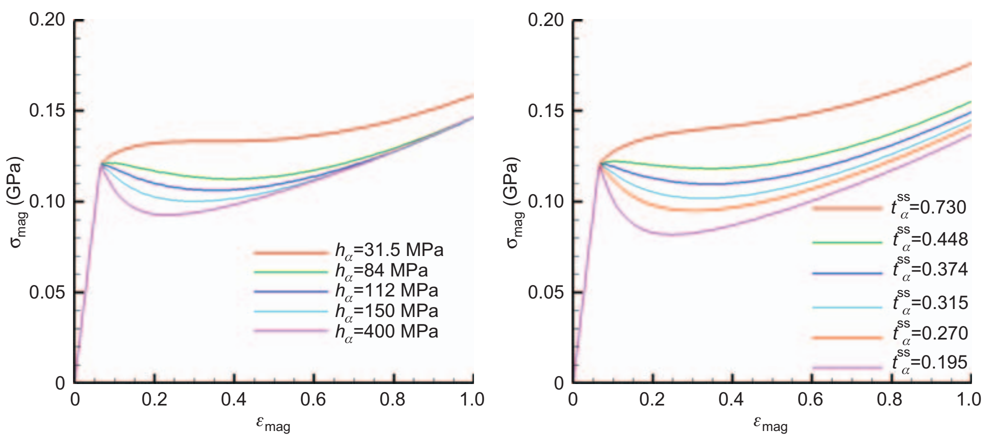

Figure 19 The σ_{mag} vs. ε_{mag} curves for different values of h_α (left) and t_α^{ss} (right) in uniaxial compression at a nominal axial strain rate of 5000/s.

Table 6 Values of the softening modulus for different values of h_α and t_α^{ss} in uniaxial compression and tension tests at nominal axial strain rates of 2000, 5000 and 7000/s.

h_α (MPa)	t_α^{ss}	Softening modulus (MPa)					
		Strain rate = 2000/s		Strain rate = 5000/s		Strain rate = 7000/s	
		Tension	Compression	Tension	Compression	Tension	Compression
31.5	0.330	-26	3	-29	0	-30	0
64.0	0.330	25	31	13	25	13	23
84.0	0.330	71	63	58	49	49	43
99.5	0.330	105	93	95	75	84	68
112.0	0.330	137	122	123	102	114	94
133.0	0.330	197	187	177	150	167	146
150.0	0.330	247	252	238	200	222	184
166.0	0.330	310	316	303	250	290	245
218.0	0.330	501	555	463	454	434	409
257.0	0.330	691	771	750	693	696	648
125.0	0.540	-4	4	-14	0	-16	-2
125.0	0.448	52	42	35	25	25	20
125.0	0.401	80	68	70	50	59	41
125.0	0.374	119	98	100	77	90	67
125.0	0.351	154	125	130	103	117	97
125.0	0.315	213	193	194	167	184	155
125.0	0.290	264	258	261	210	251	210
125.0	0.270	316	322	310	275	298	271
125.0	0.231	452	494	437	463	414	451
125.0	0.195	770	775	794	711	710	677

reference temperature of 300 K. In every case, the strain localization initiated first at a point near the circular void and the deformation localization initiation times depend noticeably upon the value of E_s. The localization initiation times at points away from the void computed for two different materials with nearly the same value of E_s but different values of h_α and t_α^{ss} varied by approximately 10%. An increase in the value of E_s from that of the PC affects the localization initiation time at a point weakly because when E_s is increased by a factor of 5 the localization initiation time at point 5 decreased by only 32%. However, a decrease in the value of E_s from that of the PC has a significant effect on the deformation localization initiation time. Near the void tip (i.e., point 1) deformations are singular and the variation with E_s of the localization time is erratic.

For the eight values of E_s, the average speed of propagation of the strain localization band listed in Table 8 reveals that the speed of propagation increases monotonically with an increase in the value of E_s; entries in the shaded row are for the PC.

Table 7 Localization initiation times at the five points of interest for different values of the softening modulus in uniaxial compression at nominal axial strain rate of 5000/s and reference temperature of 300 K; '-' indicates that the localization condition was not satisfied at the point, and the row shaded in grey corresponds to material parameters for the PC used in simulation 1.

Softening parameters (h_α[MPa], t_α^{ss})	Softening modulus (MPa)	Point 1 (μs)	Point 2 (μs)	Point 3 (μs)	Point 4 (μs)	Point 5 (μs)
(125.0, 0.330)	125.0	4.40	14.31	16.32	17.96	18.68
(125.0, 0.540)	0	4.24	–	–	–	–
(31.5, 0.330)	0	5.02	–	–	–	–
(125.0, 0.448)	25	4.10	23.53	–	–	–
(64.0, 0.330)	25	5.02	25.34	–	–	–
(84.0, 0.330)	49	3.70	19.41	31.70	–	–
(125.0, 0.401)	50	4.06	17.97	28.77	–	–
(99.5, 0.330)	75	3.40	16.61	21.75	28.30	–
(125.0, 0.374)	77	4.09	16.44	21.42	26.31	28.84
(112.0, 0.330)	102	4.72	15.40	18.63	21.61	22.68
(125.0, 0.351)	103	4.09	15.46	18.46	21.18	22.07
(133.0, 0.330)	150	3.40	13.44	15.18	16.64	17.30
(125.0, 0.315)	167	4.06	13.48	14.85	16.13	16.58
(150.0, 0.330)	200	3.43	13.11	14.21	15.66	16.33
(125.0, 0.290)	210	4.16	13.04	14.18	15.37	15.81
(166.0, 0.330)	250	3.28	12.58	13.50	14.58	15.05
(125.0, 0.270)	275	4.06	12.41	13.27	14.35	14.74
(218.0, 0.330)	454	5.01	11.60	12.26	12.73	13.13
(125.0, 0.231)	463	4.06	11.66	12.26	12.97	13.85
(257.0, 0.330)	693	4.47	11.25	11.79	12.37	12.68
(125.0, 0.195)	711	4.05	11.06	11.66	12.23	12.71

5.1.9. Effect of the shape of the geometric defect We study strain localization in the PC plate with the softening modulus equal to 25, 50, 75, 103 and 125 MPa and through-the-thickness elliptic voids with $a/b=8$, 6, 4, 2, 1/2, 1/4, 1/6 and 1/8 with the length of the major axis equal to 0.08 mm. Values of the softening modulus correspond to those found from simulations of uniaxial compression tests at a nominal axial strain rate of 5000/s with the initial temperature = 300 K. Recall that a strain localized band formed in the square plate with the circular void (i.e., $a/b=1$) for E_s equal to 77, 103 and 125 MPa but not for E_s equal to 75, 50 and 25 MPa. The localization initiation times at two points, one near the tip of the void and the other at the edge of the plate on the plane $X_3=0.002$ mm are listed in Table 9. The plane $X_3=0.002$ mm passes through integration points of all elements with one surface on the plane $X_3=0$. Coordinates of points 1 and 2 in the reference configuration are (b, 0, 0.002) and (1.0, 0.55, 0.002). For small values of a/b, the localization initiated at point 1 at the same time for all values of E_s. However, for large values of a/b the localization initiation time at point 1 increased with an increase in the value of E_s possibly due

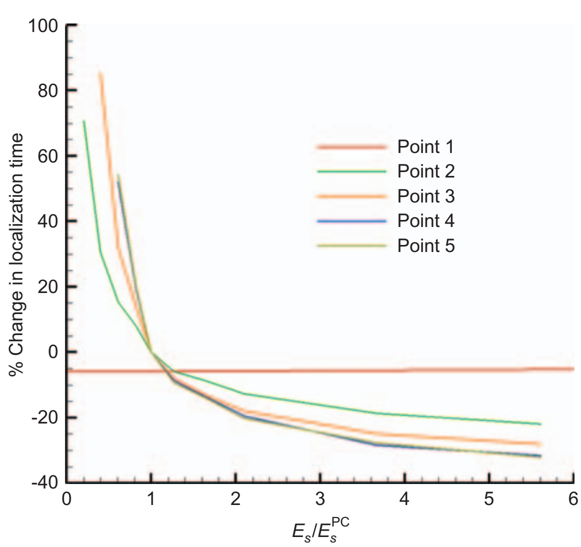

Figure 20 For the five points of interest, the percentage change in the localization initiation time compared to that of the PC vs. the ratio of the softening modulus to that of the PC; curves for points 4 and 5 overlap.

Table 8 Variation with the softening modulus of the band propagation speed in a square plate deformed in tension at a nominal axial strain rate of 5000/s. The grey filled row corresponds to the PC.

Softening modulus (MPa)	Average speed (m/s)
76.0	44.70
102.5	61.57
125.0	77.49
158.5	83.99
205.0	90.35
262.5	98.75
458.5	124.57
702.0	131.23

Table 9 Localization initiation times at a point near the elliptic void for different values of *a/b* and of the softening modulus; '–' indicates that the strain localization condition was not satisfied. Numbers in the column shaded in grey correspond to the PC.

a/b	Localization initiation time (μs)									
	E_s = 125 MPa		E_s = 103 MPa		E_s = 75 MPa		E_s = 50 MPa		E_s = 25 MPa	
	Pt – 1	Pt – 2	Pt – 1	Pt – 2	Pt – 1	Pt – 2	Pt – 1	Pt – 2	Pt – 1	Pt – 2
1/8	2.08	20.45	2.08	–	2.08	–	2.08	–	2.08	–
1/6	2.08	20.11	2.08	31.20	2.08	–	2.08	–	2.08	–
1/4	2.29	19.90	2.34	25.72	2.30	–	2.31	–	2.25	–
1/2	3.05	18.52	3.05	23.64	3.05	–	3.05	–	3.05	–
1	4.40	18.68	4.09	22.07	3.40	–	4.06	–	5.02	–
2	5.61	–	5.61	–	5.47	–	6.13	–	5.59	–
4	10.03	–	10.01	–	9.76	–	10.04	–	10.19	–
6	11.46	–	11.59	–	11.93	–	12.95	–	14.42	–
8	–	–	–	–	15.56	–	19.99	–	42.53	–

to the change in the order of singularity of deformations at point 1. Furthermore, a band of strain localization was not observed for elliptic voids with *a/b* greater than 2.0 for all values of E_s considered here. For E_s<~75 MPa, the band did not propagate to the edge of the plate for all values of *a/b*. For *a/b*=8, deformations at the point near the tip of the void did not meet the strain localization criterion for E_s=125 and 100 MPa, whereas the deformation at the same point localized for E_s=75, 50 and 25 MPa. With an increase in the value of *a/b*, the time of initiation of localization at the point near the void increased but that at the point near the edge of the plate decreased.

The average speeds of propagation of the strain localized band for different values of *a/b* and of E_s are listed in Table 10. For the same value of E_s, the maximum speed of propagation occurred for a circular void (*a/b*=1.0) even though the strain localization initiated earlier for voids with *a/b*<1.0. Whereas the localization initiated earlier for a plate with a lower value of *a/b*, the strain localized band propagated slowly because the hardening of the material also initiated early.

Figure 21 shows time histories of σ_{mag} at two points within the PC plate: (1) near the tip of the void and (2) at a distance of 0.28 mm from the void tip but within the strain localized band. It can be seen that for different aspect ratios, *a/b*, of the elliptic void, the time history of σ_{mag} is essentially the same at the point farther away from the void; however, at the tip of the void, values of *a/b* strongly influence the evolution of σ_{mag}. Thus the effect, if any, of the singularity in deformations near the void tip does not affect the evolution of stresses at a point 0.28 mm away from the void. The rate of evolution of σ_{mag} near the void tip increases with a decrease in the value of *a/b*.

Table 10 Band propagation speed for different values of *a/b* and of the softening modulus; '–' indicates that a band did not propagate to the left edge of the plate.

a/b	Band propagation speed (m/s)			
	E_s = 125 MPa	E_s = 103 MPa	E_s = 75 MPa	E_s = 50 MPa
1/8	60.21	–	–	–
1/6	61.35	37.98	–	–
1/4	62.86	47.32	–	–
1/2	71.52	53.74	–	–
1	77.49	61.57	–	–

5.2. Results for plane strain shear deformations of the plate

For the plate shown in Figure 3, we set L=1 mm, v_0=2.5 m/s and t^0=1 μs, thus the steady state nominal shear strain rate equals 5000/s. Fringe plots of ε_{mag} at t=20, 25, 35 and 45 μs for a PC with E_s=400 MPa and θ^{def}=320 K displayed in Figure 22 reveal that there is a region of high strain near the defect that propagated along the X_1-axis. Magnitudes of the shear and the axial strains within the strain localized region were found to be comparable to each other. Deformations are singular near the four corners of the plate where high values of ε_{mag} occur and propagate into the specimen interior.

5.2.1. Effect of the softening modulus In order to study the effect of the softening modulus on the propagation of the strain localization region, two points along the band of localized deformations are identified. Their locations and coordinates in the reference configuration are given in Figure 23, which shows only the left half of the plate. Point 1 is near the corner of the defect and point 2 ~0.5 mm from point 1. Note that the distance between points 1 and 2 is less than that between the points 1 and 5 in the previous problem.

The localization initiation times at the two points and the average speed of propagation of the band in the reference configuration for materials with different values of E_s are listed in Table 11. The band did not propagate to point 2 for materials with values of E_s <250 MPa; the localization initiation time decreased and the speed of propagation increased with an increase in the value of E_s.

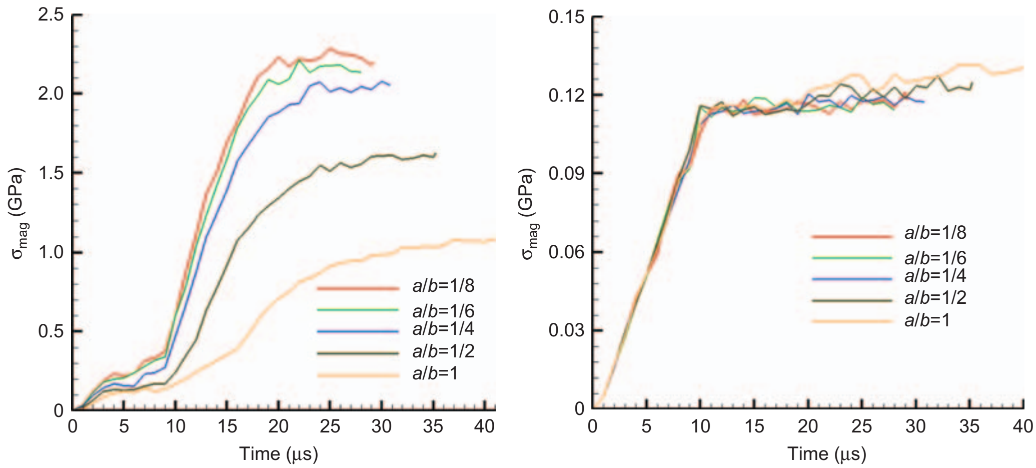

Figure 21 Time histories of σ_{mag} at (b, 0, 0.02) (left) and (0.29, 0.12, 0.02) (right) during deformations of the PC plate at the nominal axial strain rate of 5000/s.

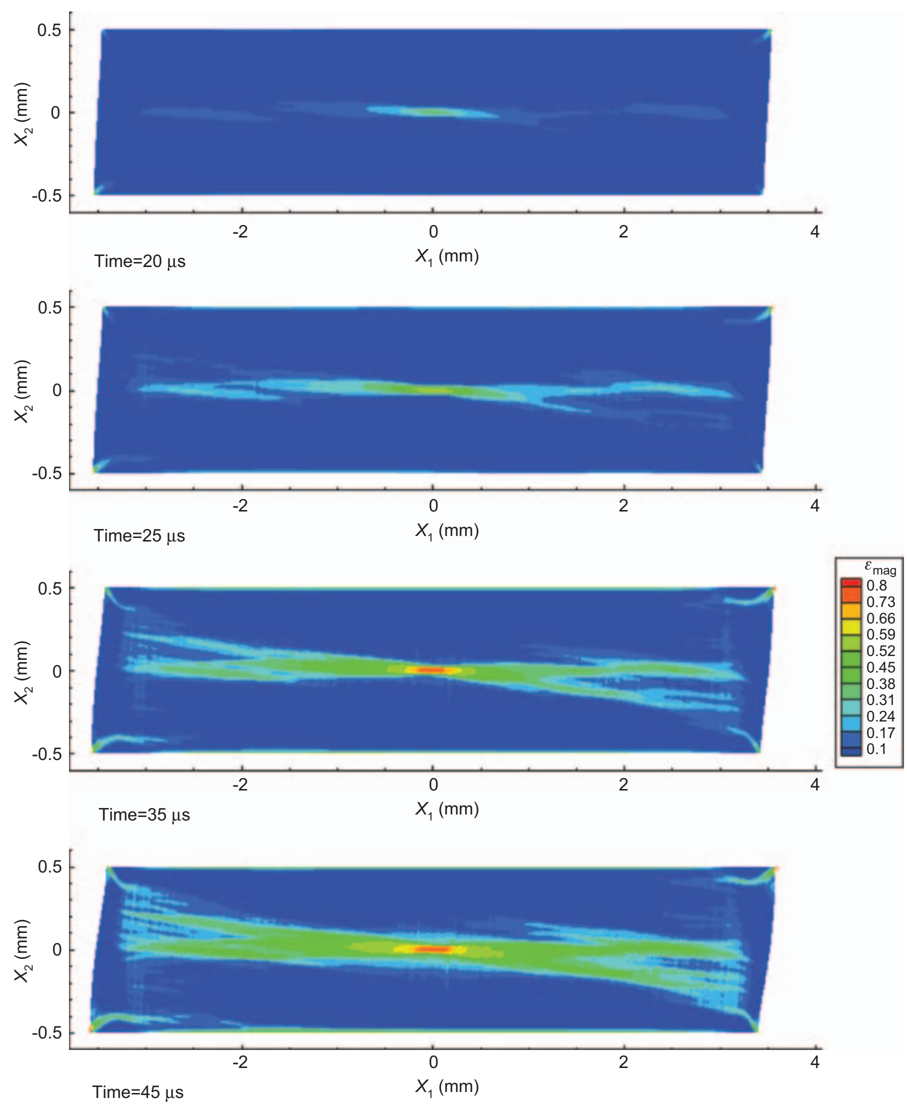

Figure 22 Fringe plots of ε_{mag} for the PC plate deformed in plane strain shear at a nominal strain rate of 5000/s at t=20, 25, 35 and 45 μs.

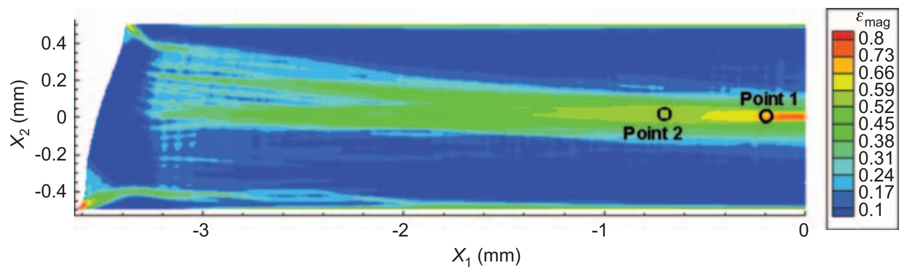

Figure 23 The location of points 1 and 2 where the localization initiation times are computed for the problem depicted in Figure 3; coordinates of points 1 and 2 in the reference configuration are (-0.194, 0.006) and (-0.694, 0.019), respectively.

5.2.2. Effect of defect strength The defect strength is varied by changing its temperature. For E_s equal to 463, 275, 210, 167 and 125 MPa and θ^{def} equal to 310, 315, 325, 330 and 350 K, the localization initiation times at points 1 and 2 listed in Table 12 imply that for materials with E_s=167 and 125 MPa, the localized deformations did not propagate from point 1 to point 2. At point 1, the localization initiation time decreased with an increase in the value of the softening modulus E_s; the same trend holds for point 3.

The speeds of propagation of the strain localized band for different values of θ^{def} and E_s are given in Table 13. For all values of θ^{def} considered here, the speed of propagation of the strain localized band increased monotonically with an increase in the value of E_s but did not increase monotonically with an increase in the temperature of the defect. The softening modulus of a PC depends on the effective plastic strain rate and the temperature of the material. Because material points of the plate are at different temperatures there is a discontinuity in E_s across the defect boundaries and that could affect the strain localization initiation time. For materials with a value of E_s less than or equal to 167 MPa, the strain localized band did not propagate.

Table 11 Strain localization initiation times at the two points exhibited in Figure 23. '–' indicates that the strain localization condition was not satisfied at the point and the row shaded in grey corresponds to material parameters for the PC.

Softening parameters (h_α[MPa], t_α^{ss})	Softening modulus (MPa)	Localization initiation times (μs)		Speed of propagation (m/s)
		Point 1	Point 2	
(125.0, 0.330)	125	27.87	–	–
(112.0, 0.330)	102	33.97	–	–
(125.0, 0.351)	103	35.39	–	–
(133.0, 0.330)	150	26.58	–	–
(125.0, 0.315)	167	26.51	–	–
(150.0, 0.330)	200	23.32	–	–
(125.0, 0.290)	210	22.79	–	–
(166.0, 0.330)	250	21.33	–	–
(125.0, 0.270)	275	20.73	27.83	70.44
(218.0, 0.330)	454	18.37	21.55	157.18
(125.0, 0.231)	463	17.25	19.46	227.13
(125.0, 0.195)	711	17.81	19.18	366.31

5.3. Results for plate with through-the-thickness circular thermal defect

We compare the localization of deformations in plates with circular through-the-thickness temperature defects with that studied above to help differentiate strain localization in shearing and tensile deformations for similar defects and identity the relative strength of thermal defects and voids. For the problems studied in this subsection we set L=1 mm, v_0= 5.0 m/s, radius of the circular region=0.04 mm and t^0=1 μs. Therefore, the steady state nominal axial strain rate equals 5000/s.

Deformations are examined for PC plates with E_s=463, 275, 210 and 125 MPa and $\Delta\theta^{def}$=30, 40, 50 and 60 K, where $\Delta\theta^{def}$ equals the temperature rise within the circular region over that in the rest of the body. A strain localized band was observed only when E_s and $\Delta\theta^{def}$ equaled 463 MPa and 60 K, respectively. Fringe plots of ε_{mag} for this case and for $\Delta\theta^{def}$= 50 K plotted in Figure 24 at times t=15, 20 and 25 μs reveal that a band of localized deformation propagated in the material for $\Delta\theta^{def}$=60 K but not for $\Delta\theta^{def}$=50 K. Thus, there appears to be a minimum value of $\Delta\theta^{def}$ below which the localized deformation does not propagate into the body.

5.3.1. Comparison with a PC plate containing a circular void For the PC with E_s=463 MPa and $\Delta\theta^{def}$=60 K the localization initiation condition was satisfied at the five points in Figure 17 at t=9.74, 13.82, 14.51, 14.65 and 14.77 μs, respectively. Comparing these times with those in the row corresponding to E_s=463 MPa in Table 7, it is clear that the strain localization criterion was satisfied later at identical points in the plate with a temperature defect than that in a plate with a circular void. Furthermore, the strain localization criterion was not satisfied at points 2, 3, 4 and 5 for plates studied here except when E_s and $\Delta\theta^{def}$ were 463 MPa and 60 K, respectively. This suggests that a thermal defect with $\Delta\theta^{def}$<60 K is weaker than a void for the PC plate studied here. The average speeds of propagation of the band in a PC plate with E_s=463 MPa with circular cylindrical void and an identical region of $\Delta\theta^{def}$=60 K are 78 and 223 m/s, respectively.

Table 12 Localization initiation times at points 1 and 2 near the defect shown in Figure 23 for different values of E_s and of the temperature of the material within the defect; '–' indicates that the strain localization condition was not satisfied and the column shaded in grey corresponds to material parameters for the PC.

θ^{def} (K)	Localization initiation time (μs)									
	E_s=463 MPa		E_s=275 MPa		E_s=210 MPa		E_s=167 MPa		E_s=125 MPa	
	Pt – 1	Pt – 2	Pt – 1	Pt – 2	Pt – 1	Pt – 2	Pt – 1	Pt – 2	Pt – 1	Pt – 2
310	20.29	22.58	24.63	–	28.81	–	–	–	–	–
315	19.30	22.18	21.80	–	24.68	–	28.60	–	34.96	–
320	17.25	19.46	20.73	27.83	22.79	–	26.51	–	27.87	–
325	17.71	20.99	19.61	26.00	21.05	–	22.62	–	24.79	–
330	17.54	19.54	19.18	23.70	20.46	–	21.90	–	22.98	–
340	17.30	19.94	17.96	24.27	19.20	–	20.37	–	21.42	–
350	17.78	19.22	18.54	22.65	18.35	26.91	19.07	–	19.90	–
360	16.44	19.15	17.05	22.80	18.42	25.84	18.52	–	19.25	–

Table 13 Band propagation speed for different values of the temperature rise of the material within the defect and of the softening modulus; '–' indicates that a band did not form.

Softening modulus (MPa)	Band propagation speed (m/s)							
	10 K	15 K	20 K	25 K	30 K	40 K	50 K	60 K
463	218	173	227	152	250	189	346	185
275	–	–	70	78	111	79	122	87
210	–	–	–	–	–	–	58	67

As for plates with voids, in plates with temperature defects deformed in tension bands of localized strain have high stretches rather than high shear strains.

5.3.2. Comparison with PC containing temperature defect deformed in plane strain shear In plates with $\Delta\theta^{def}$=60 K undergoing plane strain shearing deformations, a band was observed for E_s greater than or equal to 210 MPa as opposed to E_s=463 MPa in plates deformed in tension. Furthermore, for E_s=210 MPa, a band propagated in the plate as listed in Table 13. Thus, a band forms more readily in plates deformed in shear than those deformed in tension.

5.4. Remarks

For PC plates containing a through-the-thickness void we have not studied compressive and shearing deformations because one needs to use a contact algorithm for avoiding interpenetration of the material when the void closes. The software LS-DYNA has several contact algorithms but computed results depend upon values assigned to the penalty parameters.

Computed results have not been compared with the test data because none is available at the strain rates considered here. As evidenced by computed results, the localization of deformation strongly depends upon the type and the strength of the defect. In general, a properly oriented sharp elliptic void facilitates the localization of deformation into narrow regions. It is possible that for a very strong defect such as a notch the deformation could localize even when E_s equals zero, e.g., see entries in rows two and three of Table 7. This provides at least a partial explanation of Lu and Ravi-Chandar's [11] computing strain localization in the absence of the material exhibiting strain softening.

An experimentalist usually decides whether or not deformations have localized through either post-mortem examination of tested specimens or *in-situ* observations made on the bounding surfaces. The present analysis of transient 3D deformations reveals that deformations first localize at a point in the specimen interior, which cannot be easily detected experimentally. Also, the deformation localization criterion adopted here cannot be verified through observations made during the tests, especially at high strain rates because deformations localize in a few microseconds. Ravi-Chandar et al. [27] have used a slightly modified version of Kalthoff's experimental set-up to study the failure mode transition from a brittle crack at low impact speeds to shear banding at high impact speeds in pre-notched PC and PMMA plates impacted on a side by a cylindrical projectile of diameter equal to the plate thickness. Using high speed photography they could find the time of shear band initiation. One could potentially simulate their experimental set-up to delineate whether or not the constitutive relations proposed herein will accurately predict the shear banding in a PC plate.

Because of the nonlinear dependence of the elastic moduli upon the present temperature it is difficult to quantify the effect of the initial thermal defect upon the deformation localization. Other ways of introducing inhomogeneity include a material region with enhanced softening or lower value of the maximum stress just before the onset of strain softening; these have not been studied here.

We note that during plane strain deformations of a plate, particles are assumed to move only in the plane of the plate and displacements do not depend upon their position along

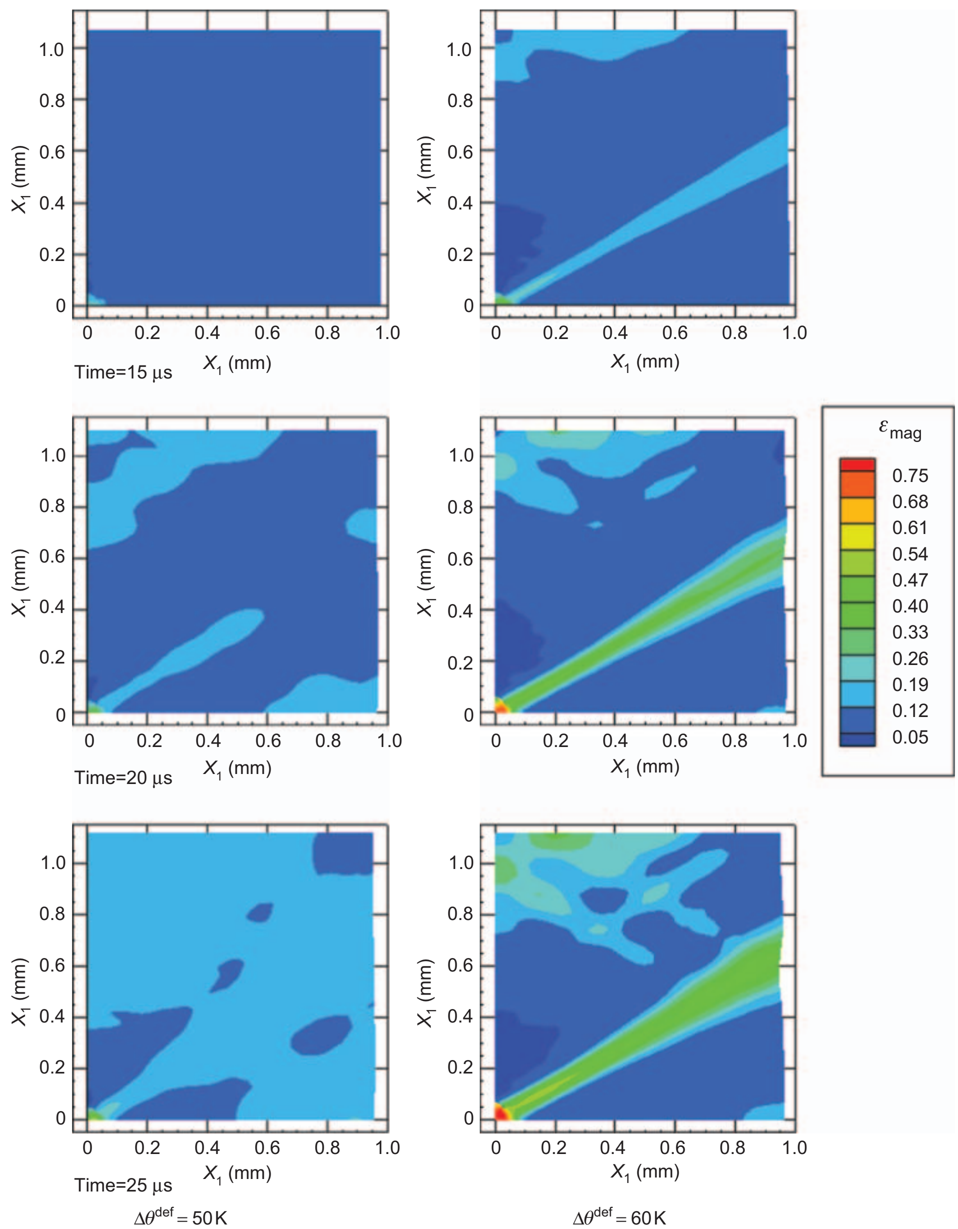

Figure 24 Fringe plots of ε_{mag} for plates with a circular cylindrical defect at $t=15$, 20 and 25 µs with initial temperature of 350 and 360 K.

the plate thickness. This assumption is reasonable only when the plate thickness is very large as compared to the other two dimensions of the plate. For a very thin plate (i.e., thickness much smaller than the plate width and the plate length) with major surfaces unloaded it is reasonable to assume that a plane state of stress prevails in the plate, i.e., $\sigma_{13}=\sigma_{23}=\sigma_{33}=0$. The usual procedure to analyze a plane stress problem is to solve the equation $\sigma_{33}=0$ for F_{33} in terms of F_{11}, F_{12} and F_{22}, and substitute for F_{33} in constitutive relations for σ_{11} and σ_{22}. For a nonlinear problem like the one being studied here, this is not feasible. Thus the assumption of plane stress does not reduce the number of unknowns and thereby simplify the analysis. Also, a thin plate deformed in shear could buckle and thus complicate the analysis of the problem. For moderately thick plates one needs to study their 3D deformations. Both plane stress and plane strain analyses provide results that agree well with test observations provided that the thickness is appropriate. Nevertheless, they help assess with less computational resources the sensitivity of results to various material and geometric parameters.

For metals, Batra and Chen [24] and Batra and Kim [28] have scrutinized the effect of different thermo-elasto-visco-plastic relations on the deformations during the pre-localization and post-localization phases. They found that different constitutive relations calibrated against the same test data predict different times of initiation of the shear band and the band width.

6. Conclusions

We have analyzed transient coupled thermo-mechanical deformations of a square PC plate deformed either in tension or in shear. In the former case, the plate has either a through-the-thickness elliptic void or a circular cylindrical region of temperature higher than that of the rest of the plate. For studying plane strain shear deformations, the plate has either a rectangular or a circular region of temperature higher than that of rest of the plate. The plate material exhibits strain softening followed by strain hardening. Effects of nominal strain rates, aspect ratios of elliptic voids, temperature rise in the defect region and values of softening parameters on the localization of deformation have been delineated.

It is found that for the same values of material parameters and defect sizes, a band forms at a lower value of the temperature rise in the defect for plates deformed in shear than those deformed in tension. For the former case the maximum principal stretch nearly equals the maximum shear strain within the band. In the latter case, the maximum principal stretch is much greater than the maximum shear strain.

For plates with a through-the-thickness elliptic void, the regions of localized deformation in the plate deformed in tension at the nominal axial strain rate of 1/s is different from that in the plate deformed at the nominal axial strain rate of 5000/s and the band width was lower in the former case than that in the latter case.

We have introduced a material property, the softening modulus E_s, to characterize the initiation of the band. E_s is defined as the minimum slope during strain softening of the magnitude of the Cauchy stress tensor vs. the magnitude of the true strain tensor curve for the PC deformed in uniaxial compression. It is found that the minimum value of E_s needed for the deformations to localize depends upon the nominal strain rate, whether the plate is deformed in tension or shear, the type of the defect (void vs. the temperature rise) and for a given defect size upon the strength of the defect. For the PC plate with a through-the-thickness void, the nominal axial strain increases with an increase in the applied nominal axial strain rate.

Acknowledgements

This research was sponsored by the Army Research Laboratory and was accomplished under Cooperative Agreement Number W911NF-06-2-0014. The views and conclusions contained in this document are those of the authors and should not be interpreted as representing the official policies, either expressed or implied, of the Army Research Laboratory or the U.S. Government. The U.S. Government is authorized to reproduce and distribute reprints for Government purposes notwithstanding any copyright notation herein.

AGV would also like to thank Dr. Kaushik Das, Dr. Shakti Gupta and Mr. Gautam Gopinath for their valuable input on the subject.

Appendix A

Algorithm for the user-defined material subroutine umat41

subroutine umat41($\boldsymbol{\sigma}$, $\mathbf{D}$, $\mathbf{F}$, $\mathbf{F}^{\mathbf{p}}_{\alpha}$, $\mathbf{F}^{\mathbf{p}}_{\beta}$, t_α, t_β, θ, t, Δt)

//Compute Cauchy stress tensor at time $t+\Delta t$

$\dot{\varepsilon}=\mathrm{tr}(\mathbf{DD})$

$[E_\alpha, E_\beta]=$Compute_Youngs_Modulus($\dot{\varepsilon}$, θ)

for $i=\alpha,\beta$

$$\mathbf{F}^{\mathbf{e}}_{\alpha}=\mathbf{F}\,(\mathbf{F}^{\mathbf{p}}_{\alpha})^{-1};\ J_i=\det(\mathbf{F}^{\mathbf{e}}_{i});\ \mathbf{V}^{\mathbf{e}}_{\alpha}=[\mathbf{F}^{\mathbf{e}}_{\alpha}(\mathbf{F}^{\mathbf{e}}_{\alpha})^{\mathrm{T}}]^{1/2}$$

$$\lambda_i=\frac{E_i(1+\nu_i)}{2},\ \mu_i=\frac{E_i}{2(1+\nu_i)}$$

$$\boldsymbol{\sigma}_i=\frac{1}{J_i}\left[2\mu_i\ln\mathbf{V}^{\mathrm{e}}_i+\lambda_i\mathrm{tr}(\ln\mathbf{V}^{\mathrm{e}}_i)\boldsymbol{\delta}\right]$$

end for

$$\bar{\mathbf{B}}_{\mathrm{B}}=(\det\mathbf{F})^{-2/3}\mathbf{F}\mathbf{F}^{\mathrm{T}};\ \lambda^{\mathrm{p}}=\sqrt{\mathrm{tr}\left(\bar{\mathbf{B}}_{\mathrm{B}}\right)/3}$$

$$\boldsymbol{\sigma}_{\mathrm{B}}=\frac{C_{\mathrm{R}}}{3}\frac{\sqrt{N_l}}{\lambda^{\mathrm{p}}}L^{-1}\left(\frac{\lambda^{\mathrm{p}}}{\sqrt{N_l}}\right)\bar{\mathbf{B}}'_{\mathrm{B}}$$

$$\boldsymbol{\sigma}=\boldsymbol{\sigma}_\alpha+\boldsymbol{\sigma}_\beta+\boldsymbol{\sigma}_{\mathrm{B}}$$

//Compute rate of $\mathbf{F}^{\mathbf{p}}_{\alpha}$, $\mathbf{F}^{\mathbf{p}}_{\beta}$, t_α, t_β, and θ at time $t+\Delta t$

for $i=\alpha, \beta$

$$\hat{s}_i=0.077\mu_i/(1\text{-}\nu_i);\ \tau_i=\sqrt{0.5\mathrm{tr}\left(\boldsymbol{\sigma}'_i\boldsymbol{\sigma}'_i\right)};\ p=\text{-}\boldsymbol{\sigma}_{ii}/3$$

$$\dot{\gamma}^{\mathrm{p}}_i=\min\left(\dot{\gamma}^{\mathrm{p}}_{0i}\exp\left[\text{-}\frac{\Delta G_i}{k\theta}\left(1\text{-}\frac{\tau_i}{t_i\hat{s}_i+\alpha^{\mathrm{p}}_i p}\right)\right], 10^5/\mathrm{s}\right)$$

$$\dot{t}_i=\frac{h_i}{\hat{s}^0_i}\left(1\text{-}\frac{t_i}{t^{\mathrm{ss}}_i}\right)\dot{\gamma}^{\mathrm{p}}_i$$

$$\tilde{\mathbf{D}}^{\mathrm{p}}_i=\dot{\gamma}^{\mathrm{p}}_i\frac{\boldsymbol{\sigma}'_i}{|\boldsymbol{\sigma}'_i|}$$

$$\dot{\mathbf{F}}^{\mathrm{p}}_i=\mathbf{F}^{\mathrm{e}^{-1}}_i\tilde{\mathbf{D}}^{\mathrm{p}}_i\mathbf{F}_i$$

end for

$$\dot{\theta}=(1/\rho_0 c)\left[J_\alpha\mathrm{tr}\left(\boldsymbol{\sigma}_\alpha\tilde{\mathbf{D}}^{\mathrm{p}}_\alpha\right)+J_\beta\mathrm{tr}\left(\boldsymbol{\sigma}_\beta\tilde{\mathbf{D}}^{\mathrm{p}}_\beta\right)\right]$$

//Compute $\mathbf{F}^{\mathbf{p}}_{\alpha}$, $\mathbf{F}^{\mathrm{p}}_{\beta}$, t_α, t_β, and θ at time $t+\Delta t$

for $i=\alpha,\beta$

$$\mathbf{F}^{\mathrm{p}}_i=\mathbf{F}^{\mathrm{p}}_i+\dot{\mathbf{F}}^{\mathrm{p}}_i\Delta t$$

$$t_i=t_i+\dot{t}_i\Delta t$$

$$\theta=\theta+\dot{\theta}\Delta t$$

end for

end subroutine

Here $\mathbf{D}$ is the strain rate tensor, t is the current time, and Δt is the value of the current time step computed by LS-DYNA. Values of variables $\boldsymbol{\sigma}$, $\mathbf{D}$, $\mathbf{F}$, $\mathbf{F}^{p}{}_{\alpha}$, $\mathbf{F}^{p}{}_{\beta}$, t_{α}, t_{β}, and θ at time t are passed as input to the subroutine umat41. The subroutine then return values of $\boldsymbol{\sigma}$, $\mathbf{F}^{p}{}_{\alpha}$, $\mathbf{F}^{p}{}_{\beta}$, t_{α}, t_{β}, and θ at time $t+\Delta t$ back to LS-DYNA as directed in the above Algorithm.

A technique to verify that the computer code correctly solves an initial-boundary-value problem is described in the text following Eq. (20) of [30]. The constitutive relation employed here is similar to that used in [31] in the sense that there is no explicit yield surface to delineate loading/unloading at a material point.

References

[1] Meijer HEH, Govaert LE. *Prog. Polym. Sci.* 2005, 30, 915–938.
[2] Mulliken AD, Boyce MC. *Int. J. Solids Struct.* 2006, 43, 1331–1356.
[3] Ward IM. *Mechanical Properties of Solid Polymers*, 2nd ed. Chichester: Wiley, 1983.
[4] Haward R,Young R. *The Physics of Glassy Polymers*, 2nd ed. London: Chapman & Hall, 1997.
[5] Buisson G, Ravi-Chandar K. *Polymer* 1990, 31, 2071–2076.
[6] G'Sell C, Boni S, Shrivastava S. *J. Mater. Sci.* 1983, 18, 903–918.
[7] Wu W, Turner APL. *J. Polym. Sci. A2* 1973, 11, 2199–2208.
[8] G'Sell C, Gopez AJ. *J. Mater. Sci.* 1985, 20, 3462–3478.
[9] Neale KW, Tugcu P. *J. Mech. Phys. Solids* 1985, 33, 323–337.
[10] Grenet J, G'Sell C. *Polymer* 1990, 31, 2057–2065.
[11] Lu J, Ravi-Chandar K. *Int. J. Solids. Struct.* 1999, 36, 391–425.
[12] Wu PD, van der Giessen E. *Int. J. Solids Struct.* 1994, 31, 1493–1517.
[13] Tomita Y, Takahashi T, Shindo A. *Int. J. Mech. Sci.* 1990, 32, 335–343.
[14] Boyce MC, Parks D, Argon A. *Mech. Mater.* 1988, 7, 15–53.
[15] Wu PD, van der Giessen E. *Int. J. Plasticity* 1995, 11, 211–235.
[16] Sweeney J, Caton-Rose P, Spares R, Coates PD. *J. Appl. Polym. Sci.* 2007, 106, 1095–1105. DOI: 10.1002/app.26546.
[17] Govaert LE, Timmermans PHM, Brekelmans WAM. *J. Eng. Mater. Technol.* 2000, 122, 177–185.
[18] Batra RC, Kim CH. *Int. J. Eng. Sci.* 1991, 29, 949–960.
[19] Varghese AG, Batra RC. *Int. J. Solids Struct.* 2009, 46**,** 4079–4094.
[20] Varghese AG. Strain localization in tungsten heavy alloys and glassy polymers. Ph.D. Dissertation. Virginia Polytechnic Institute and State University: Blacksburg, VA, 2008.
[21] Lee EH. *J. Appl. Mech.* 1969, 36, 1–6.
[22] Batra RC. *Int. J. Nonlinear Mech.* 2001, 36, 421–432.
[23] Mulliken AD. Low to high strain rate deformation of amorphous polymers: experiments and modeling. M.S. Thesis. Massachusetts Institute of Technology: Cambridge, 2004.
[24] Batra RC, Chen L. *Int. J. Plasticity* 2001, 17, 1465–1489.
[25] Bauwens-Crowet C, Bauwens J, Homès G. *J. Mater. Sci.* 1972, 7, 176–183.
[26] Wright TW, Walter JW. *J. Mech. Phys. Solids* 1987, 35, 701–720.
[27] Ravi-Chandar K, Lu L, Yang B, Zhu Z. *Int. J. Fracture* 2000, 101, 33–72.
[28] Batra RC, Kim CH. *J. Mech. Phys. Solids* 1990, 38, 859–874.
[29] Batra RC, Lear MH. *Int. J. Plasticity* 2005, 21, 1521–1545.
[30] Batra RC, Liang XQ. *Computational Mechanics* 1997, 20, 427–438.
[31] Batra RC, Liu DS. *Int. J. Plasticity* 1990, 6, 231–246.